NEUTRON TUNNELING IN NANOSTRUCTURED SYSTEMS: ISOTOPICAL EFFECT

By

Aphiwe Matiwane

Submitted in accordance with requirements for the degree of

MASTER OF SCIENCE

In the subject of

PHYSICS

at the

University of South Africa

Supervisor: Prof. M. Maaza

Co-supervisor: Prof. M.L. Lekala

January 2018

DECLARATION

Name: Aphiwe Matiwane

Student number: 58563008

Degree: MSc Physics

Neutron tunneling in nanostructured systems: isotopical effect

I declare that the above dissertation/thesis is my own work and that all the sources that I have used or quoted have been indicated and acknowledged by means of complete references.

Signed 15 October 2018

SIGNATURE DATE

DEDICATIONS

I dedicate this thesis to my family and friends for their words of encouragement, continued support, patience and understanding.

ACKNOWLEDGEMENTS

I would like to acknowledge my supervisor, Prof. Malik Maaza for his constant support and words of encouragement when things didn't seem to happen. His wisdom, suggestions, and guidance helped in a great deal. I would like to express many thanks and gratitude to my co-supervisor Prof. Mantile Lekala for his words of advice and encouragement during difficult times, his assistance in putting together the dissertation. I give many thanks to Prof. Alain Gibaud for his assistance with the software and suggestions. I would like to extend my gratitude to Dr. Mlungisi Nkosi for his support and assistance. I appreciate the guidance of Dr. Christopher Mtshali for his assistance and words of encouragement, Dr. Noluthando Mayedwa for her assistance in my defense proposal presentation.

I would like to thank Dr. Zebib Nuru and Dr. Sidiki for their words of support, encouragement, and help during the period of my MSc work. I would also like to thank Dr. Juliet Sackey for her help and advice. I would like to sincerely express my gratitude to Ms. Ntombizonke Kheswa for being a mentor and a mother to me during the work of my MSc. I also like to thank MRD staff, postdocs and fellow students for their advice and words of encouragement.

I'm grateful to National research foundation (NRF-SANHARP) for their financial support, the University of South Africa for allowing me to be a student in this prestigious institution and also NRF-iThemba LABS for letting me use their equipment.

My gratitude goes to my family and friends for their support and patience. Last but not least, I would like to thank each and every person who helped me one way or the other in the completion of my research work.

LIST OF ABBREVIATIONS

SLD: Scattering length density

NR: Neutron reflectometry

F-P: Fabry-Perot resonator

FTR: Frustrated total reflection

Q: Momentum wave vector transfer

FWHM: Full width at half maximum

SUMMARY

Tunneling phenomenon has been studied since the time of Sir Isaac Newton. In the case of neutron tunneling phenomenon, it is the quantum mechanics wave-particle duality which manifests itself. In this case, particularly, the neutron wave-packet under total reflection condition suffers the so-called frustrated total reflection as known in standard optics. More accurately, this tunneling phenomenon shows itself via sharp dips in the plateau of total reflection. The prerequisite to observe such quantum mechanics phenomenon lies within a thin film Fabry-Perot resonator configuration. This thin film Fabry-Perot resonator geometry consists of two reflecting mirrors separated by a transparent material from a neutron optics viewpoint. In view of the specific neutron scattering properties related to the spin of the neutron wave-packet. As a direct proof, isotopic nickel based thin films Fabry-Perot resonator have been fabricated by depositing thin film of nickel by ion beam sputtering. The vacuum chamber was pumped down to the pressure of 10^{-8} mbar and deposition was performed at pressure of $2x10^{-4}$ mbar. The deposition rate was kept at 1.5 nm / minute and thickness layers were monitored by a calibrated quartz microbalance. Unpolarized neutron reflectometry measurements were carried out at the ORPHEE reactor using the time-of-flight EROS reflectometer. The incidence neutron wavelength varied between 3 – 25 Å. The grazing angle and angular resolution were of the order of 0.8˚ and 0.05 respectively. The software program, a Matlab routine for the simulation of specular X-ray and neutron reflectivity data with matrix technique, was employed to simulate the phenomenon and thereafter the experimentally obtained data and calculated (theoretical) data were compared. From the analysis of the comparison, a conclusion was drawn about the agreement between experimental data and theoretical data. The tunneling phenomenon has been observed in nanostructured isotopic nickel based thin film Fabry-Perot resonator. It manifested itself by the existence of dips, tunneling resonances, in the total reflection plateau due to quasi-bound states in the isotopic nickel based thin film Fabry-Perot resonator. In total, there were 7 tunneling resonances. The full widths at half maximum of these dips were found to decrease with increasing momentum wave vector transfer (Q) and this correlated to the neutron lifetime in the nanostructured isotopic nickel based thin film Fabry-Perot resonator.

KEY TERMS

Neutron tunneling

Nanostructures

Tunneling resonances

Total reflection plateau

Fabry-Perot resonator

Reflectivity profile

Neutron reflectometry

Vitreous region

Kiessig fringes

Scattering length density

TABLE OF CONTENTS

TABLE OF FIGURES

LIST OF TABLES

Chapter 1

Introduction

1.1 Overview

Neutron is an uncharged, subatomic particle with a mass of 1.675×10^{-27} kg. It is 1839 times than the electron, has a spin-parity of $(\frac{1}{2})^{+}$ and a magnetic moment of -1.913 nuclear magnetons [1]. It was discovered by James Chadwick in 1932. Neutrons are stable when bound in an atomic nucleus while having a lifetime of 900 seconds as a free particle [2] .

Neutron beams are produced in two general ways: by nuclear fission in reactor-based neutron source or by spallation in accelerator-based neutron sources [3] . In the reactor-based process, thermal neutrons are absorbed by uranium-235 nuclei which split into fission fragments and evaporate at very high energy (MeV) [4]. After the high energy neutrons have been thermalized, beams are emitted with a broad wavelength [5]. Wavelength selection is generally achieved by Bragg scattering from a crystal monochromator or by velocity selection through a mechanical chopper. In this way, high quality, high flux neutron beams with a narrow wavelength distribution are made available for scattering experiments [6].

Accelerator-based pulsed neutrons are released by bombarding a heavy metal target (uranium, tantalum, and tungsten) with high energy particles (e.g. H^{+}) from a high power accelerator, a process known as spallation [7] . The methods of particles acceleration tend to produce short intense bursts of high energy protons, and hence pulses of neutrons. Spallation releases much less heat per useful neutron than fission, 30 MeV per neutrons compared with 190 MeV in fission [8].

Almost everything we know about the structure of the matter is a result of scattering experiments by whatever the type of radiations used. These are usually scattering of photons, electrons, protons, neutrons, X-rays etc. Neutron scattering is an important tool for studying condensed matter, nuclear and biological systems and neutron imaging technology which is widely used in industries. Neutron scattering provides information that is highly complementary to that of other scattering techniques [9]. Since neutron is uncharged employing it in neutron scattering makes it possible to penetrate deeper than electrons which are charged and therefore interact with the electron clouds of atoms of matter being investigated.

This brings the topic of optics, which is described as the behavior of waves, interacting with matter. Waves are characterized by their wavelength (frequency or momentum) while matter is characterized by susceptibility and the wave-matter interaction is characterized by the index of refraction from an optical viewpoint [10]. It is the neutron wave-packet that is of interest, as it goes under total reflection condition suffers the so-called total reflection as known in standard optics.

In order to determine the atomic arrangement or their magnetic interaction in bulk or nanostructured material, neutrons should be employed due to their unique properties i.e. spin, magnetic moment, uncharged, neutron decay etc. It is this set of specific properties that make neutrons to be superior probing tool for a large variety of matter [11].

Since neutrons possess the above-mentioned properties, this makes it possible to study microscopic properties of bulk or nanostructured samples [12]. As a result, neutrons can travel longer distances through most materials without being scattered or absorbed. This means that the attenuation of neutrons by matter, e.g. aluminium, is about 1% per millimeter compared to 99% per millimetre or more for X-rays [9]. They interact mainly with the nucleus and the electron clouds if the sample exhibit magnetic properties. Their magnetic moment which enables them to study materials with magnetic properties is a singular characteristic [13]. Spin-spin interaction leads to coherent scattering. In addition, considering the statistical variation of their neutron scattering cross section with the atomic number, it is possible to distinguish easily light nuclei and differentiate between isotopes at the expense of heavy nuclei [14].

Neutron beams are classified according to their wavelengths and energy. Epithermal are short wavelengths neutron beam (approximately 0.1 Å) whereas thermal and cold neutron beams are for longer wavelengths (approximately 10 Å). [15].

Neutrons with longer wavelengths are of interest in this study and there will be an observation of their movements (tunneling) within the Fabry-Perot resonator. The Fabry-Perot is a more widely used research instrument today than at any other time. Its main components are two plane mirrors of high reflectivity arranged parallel and separated by a gap [16]. Its origin derives from the theory of multibeam interferences developed by Charles Fabry in 1890-1892 and incorporated into design interferometer by Fabry and his colleague, Alfred Perot in 1897 [17]. The first prototype developed

by Fabry and Perot consisted of two flat glass plates coated on their parallel facing surfaces with thin silver films. These metal films reflected over 90% of the light incident on them. The light beam incident on the outer part of glass would pass through the silver coating and then get trapped between silver plates and reflected back and forth. At every reflection, a small fraction of the incident beam would escape through the outer surface of the second plate [18]. Modern Fabry-Perot resonators can be used at wavelengths near 500 nm, with a fixed separation of 1 cm between coated surfaces and reflectivity for the coated surfaces [19] .

The tunneling phenomenon of neutron wave-particles is observed in nanostructured systems. The interest lies in nanostructures of Fabry-Perot resonators, as the tunneling of neutrons is observed in these types of nanostructured [20-24] . A typical Fabry-Perot resonator consists of two highly reflecting mirrors separated by a transparent material as shown in Figure 1.1 [25]. The Fabry-Perot resonator is constructed by closing all 'doors' through which waves can escape [26]. One exploits the fact that transmission through such a resonator exhibits sharp resonances [27].

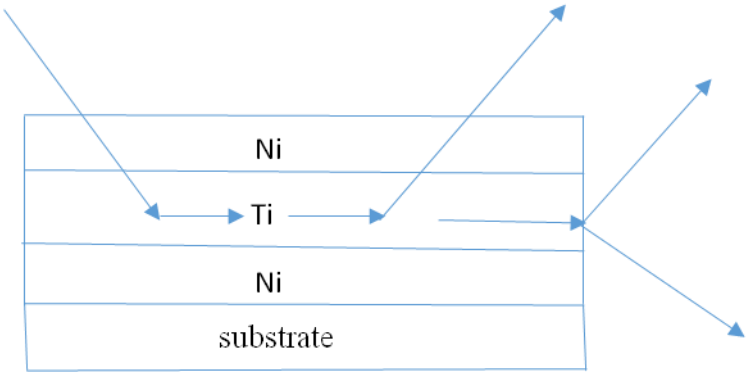

Figure 1.1: A typical nano-structured Fabry-Perot resonator used to observe tunneling phenomenon of neutron wave-particles.

1.2 Problem statement

Different elements have been used in the past in synthesis of thin film Fabry-Perot resonator such as Ni-V-Ni, Cu-Al-Cu, dPEP-PEP-dPEP [28] etc to observe this tunneling phenomenon. In the past, the focus was more on natural materials as part of constituents on the synthesis of thin film Fabry-Perot resonator. In this study, isotopes of the same elements will be employed to observe this tunneling of neutron wave-particles suffering a total reflection or frustrated reflection, in the thin film Fabry-Perot resonator and hence engineer novel neutron optics devices for neutron

research reactors. To the best of our knowledge, it will be the first time to do this study solely based on isotopes. As it is known, isotopes are similar in chemical composition (the same electron shell) and the values of the crystal grid constant but differ in physical characteristics (band gap width, nuclear spins, refraction index, absorption, etc). These differences are related to features of isotope effect. The isotope effect is caused by changes in the number of neutrons in the nucleus with a constant number of protons. The combination of different isotopes of the same chemical element makes it possible to create space limitations in nanostructures without using other chemical elements [1, 2].

In view of the difficulty associated with the synthesis of the isotopic nickel thin film Fabry-Perot resonator such as homogeneity; uniformity and roughness of the thin films, it is essential to use high volume during the deposition in order to avoid possible contamination. Good volume is achievable by having good pressure. This means low pressure around 10^{-6} mbar.

Neutrons are weakly scattered once they are inside the matter and they tend to lose intensity. It would be vital to have good intensity of neutron beam so that there's no intensity that would be lost once neutrons are interacting with the thin film Fabry-Perot resonator and therefore the tunneling of neutron wave-particle can be observed [29].

1.3 Rationale / Motivation

The purpose of the study is to observe the tunneling phenomenon of neutrons in isotopic based Fabry-Perot resonator nanostructures. To the best of our knowledge, this will be the first time that this phenomenon has been observed in isotopic based nanostructures. The study contributes in estimating neutron lifetime, Zeeman birefringence and surface/interface diamagnetism. Furthermore, it reports some potential technological application in neutron optics to make novel neutron optics devices such as monochromators, polarizers, and beam splitters. The study also looks forward to manufacturing novel neutron optics for neutron research reactors based completely on isotope based nanostructures. Using frustrated total reflection, tunneling phenomenon, in Fabry-Perot resonators could open a new perspective in the investigation of the behavior of superconductors, such as non-locality, proximity, and surface anisotropy effects.

1.4 Aims and Objectives

The aim of this research project is to observe the tunneling phenomenon of neutron wave-particles undergoing the total reflection (the 'frustrated' total reflection of neutron wave-particle) in isotopic based nickel thin films Fabry-Perot resonators. To this end, the following are the objectives of the study:

(i) To fabricate isotopic nickel thin films Fabry-Perot like resonator

(ii) To observe tunneling process of neutron wave-particle in the isotopic nickel thin films Fabry-Perot resonator by unpolarized grazing incidence neutron reflectometry.

In this study, Reflex13, which is a Matlab routine for the simulation of specular X-ray and neutron reflectivity data with matrix technique, was employed to simulate the behavior of the tunneling phenomenon. Thereafter, the experimental and simulated results were compared.

References

[1] J. Finney and S.Steignberger, *Physics World,* vol. 10, no. 12, 1997.

[2] J. Chadwick, "Possible Existence of Neutron," *Nature*, vol. 129, p. 312, 1932.

[3] S.M. King, "Small-Angle Neutron Scattering," a report publsihed on ISIS Web page, 1997.

[4] M. Kotlarchyk, S-H.Chen and J. a. M.W.Kim, *J.Phys.Chem.*, vol. 29, p. 2054, 1984.

[5] M. Born and E.Wolf, "Principles of optics," Pergamon, Oxford, 1980.

[6] L. Auvray and P.Auroy, "Neutron, X-ray and Light Scattering,," Holland, Elsevier Science Publishers, 1991.

[7] R. K.Heenan, J.Penfold and S.M.King, *J.Apply.Cryst.*, vol. 30, p. 1140, 1997.

[8] O.J. Heavens, "Optical properties of thin solid films," London, Butterworth Scientific publication, 1955.

[9] R. Pynn and W.G. Stirling and C.M.E.Zeyen, *Physica,* vol. 120B, p. 86, 1983.

[10] T. Chupp, "Neutron optics and polarization," University of Michigan.

[11] S. Anderson, S.Cook, G.P.Fletcher, T.Gentle, G.L.Greene, F.Klose, F.Koetze, A.Parizz R.J. Pynn and J.K.Zhao, *J.NeutronRes.*, vol. 13, p. 193, 2005.

[12] K. Lonsdale, "Neutron diffraction by crystals;," *Nature*, vol. 164, p. 205-209, 1949.

[13] "flnp.jinr.ru/375/," [Online].

[14] A.L. Frank, "Fundamental properties of neutron : Fifty years of research," *Sov.Phys.Usp.*, vol. 25, pp. 280-297, 1982.

[15] L. Auvray and P.Auroy, "Neutron, X-ray and Light Scattering;," Holland, Elsevier Science Publishers, 1991.

[16] J.M. Vaughan, "The Fabry-Perot interfermeter;," Bristol, Hilger, 1989.

[17] G. Hernandez, "The Fabry-Perot interferometer;," New York, Cambridge Up, 1986.

[18] A. Francis and E.Jenkins, H.E.White, "Fundamentals of optics;," New York, McGraw-Hill, p. 301-311, 1976

[19] F. Abeles, *Phys.(Paris);*, vol. 3, p. 504, 1948.

[20] P. Moriarty, "Nanostructured materials;," *Rep.Prog.Phys.*, vol. 64, 2001.

[21] H.N. Singh, "Nanostructured materials and nanotechnology;," London, Academic Press, 2002.

[22] L.M. Zhuravleva , N.M.Legkiiy,V.G.Plekhanov, "Isotopic nanostructures;," *Life Sci J.*, 2014.

[23] V.G. Plekhanov, "Isotopes in condensed matter;," Berlin, Heidelberg, Springer, 2012, p. 3-293.

[24] V.G. Plekhanov, "Giant isotope effects in solids;," USA, La Jolla stefan University Press, 2004, p. 3-187.

[25] C.h. Fabry, H. H.Perot, *Ann.Chim.Phys.*, vol. 12, p. 459, 1897.

[26] Y. Plotnik, F.Dreisow, M.Heinrich, S.Nolto and A..Szameit and M.Seger, "Experimental observation of optical bound state in the continuum.," *Phys.Rev.Lett.*, vol. 107, p. 183-187, 2011.

[27] V.K. Ignatovich and F.Radu, *Phys.Rev.*, vol. 13, no. 64, p. 205-208, 2001.

[28] L.J. Norton, E.J.Kramer, R.A.L.Jones, F.S.Bates, H.R.Brown and G.P.Fletcher, R.Kleb, *J.Phys.(Paris)*, vol. 4, no. 11, p. 367, 1994.

[29] J.R. Dunning, "Interaction of neutrons with matter;," *Phys.Rev.*, vol. 48, p. 205-280, 1935.

Chapter 2

Literature review

2.1 Nanostructures

Nanostructures refer to materials system with length scale in the range of approximately 1-100 nm in at least one dimension [1]. In nanostructures, electrons are confined in the nanoscale dimensions but are free to move in other dimensions. One way to classify nanostructures is based on the dimension namely 0D, 1D, 2D and 3D in which electrons move freely. Example of 1D include a quantum well in which electrons are confined in one dimension (1D), an example of a 2D nanostructure is the quantum wire, in which electrons are confined in two dimensions while the 3D nanostructure example is the quantum dots, where the electrons are confined in three dimensions, as shown in Figure 2.1.1, [2].

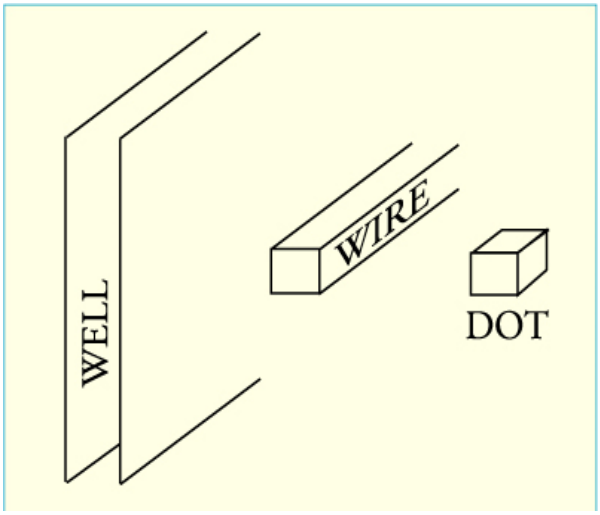

Figure 2.1.1 showing examples of nanostructures in their dimensions

Nanostructures are unique and interesting due to their properties. At nanoscale level, significant changes in property occur as opposed to the bulk. These property changes are affected by the following phenomena: quantum confinement, quantum coherence, and surface/interface effects. Quantum confinement deals with confinement of electrons in the nanoscale dimension which results in quantization of energy and momentum and reduced dimensionality of electronic states. Yet in the quantum coherence: certain phase relation of the wave function is preserved for electrons moving in a nanostructure, so wave interference effect must be considered [3]. But in

nanostructures, generally, the quantum coherence is not maintained perfectly as in the atoms and molecules. The coherence is often disrupted to some extent by defects in the nanostructures. Therefore, both quantum coherent and de-coherent effects have to be considered, which often makes the description of electronic motion in a nanostructure more complicated. In the surface/interface effects: a significant fraction, even majority of atoms in a nanostructure are located at near the surfaces or interfaces. The mechanic, thermodynamic, electronic, magnetic, optical and chemical states of these atoms can be quite different than those interior atoms [3].

Nanostructured materials are often in a metastable state. The detailed atomic configuration depends on the kinetic process in which they are fabricated; therefore the properties of nanostructures can be widely adjustable by changing their size, shape and process condition [3].

Historically it was Richard Feynman's lecture, "There's plenty of room at the bottom", that has been quoted when people talk about nanoscience and nanotechnology. He predicted that we will get an enormously greater range of properties that substances can have and of different things that we can do if atoms can be arranged in the way we want. The real take-off of nano-related research and technological exploitation started at about 15 years ago [4]. Our understanding and exploitation of material world around have been pushing forward in two opposite direction: from the top down and from bottom-up. In the bottom-up approach, material starts from electrons and nucleons as the building blocks while in the top-down approach the material is big and it is chipped down to electrons and atoms [5]. The top-down and bottom-up approaches have largely developed independently in the past [6]. Today these two meet at the nanoscale territory. This means that scientist along the top-down line have to consider the behavior of nature at the atomic scales, while those taking the bottom-up approach are ready to fabricate novel devices and materials with atoms and molecules as the building blocks [7].

In addition to nanostructures, there are isotopic nanostructures. Isotopes have the same number of protons but a different number of neutrons [8]. Since the mass number is the number of protons, isotope can also be defined as the atom with the same atomic number and different mass number. Isotopes have similar composition, that is same electron shell but different physical characteristics such as index of refraction, absorption, nuclear spins, band gap etc [9]. All these differences

contribute and are related to features of isotope effect [10]. Hence to utilize isotopic material means that there would be improved neutron optical index such as refractive index which increases the contrast. In optics, index of refraction determines the reflection and transmission of neutrons depending on the angle [49].

The neutron tunneling phenomenon is observed in these kinds of thin films Fabry-Perot resonator like nanostructures. These thin films Fabry-Perot resonators like are made up of two reflecting mirrors separated by a spacer layer (transparent layer). They are synthesized mainly by two ways: Physical vapor deposition and chemical vapor deposition.

In chemical vapor deposition: a chemical process is used to produce high-quality materials. This process is usually employed in the semiconductor industry to produce thin films. Briefly, a substrate is exposed to the material which is heated to produce the deposit [11].

The physical method provides an eco-friendly path to the synthesis of materials. Currently, there are various physical method used such as electron beam deposition, ion beam sputter technique, pulsed laser deposition, evaporative deposition etc. Ion beam sputter is when a glow plasma discharge bombards the material; evaporative deposition is when a material is heated to high vapor deposition by electrical resistance heating [12]. Pulsed laser deposition is the type of physical vapor deposition (PVD) that uses a high power laser that ablates material from the target into vapor [13]. An electron beam physical vapor deposition operates when a target anode is bombarded with an electron beam that's coming from a tungsten filament under high vacuum. Electron beam transforms atoms in the target into a gaseous phase, which precipitates into a solid form and coat the substrate. [14]. In this study, an ion beam sputtering technique was employed in synthesizing nickel isotope thin film Fabry-Perot resonator like deposited on a silicon substrate in the following sequence: 110 Å ^{58}Ni / 1000 Å ^{62}Ni / 110 Å ^{58}Ni/Si.

Ion beam sputtering technique uses ion source to produce a focused beam directed at the target to be sputtered. The ion source is made up of cathode and anode. When a high voltage field of 2-10 kV is applied to the anode it creates an electrostatic field inside the ion source. When argon is injected into the ion source, the high electric field causes the gas to ionize, creating a plasma inside the ion source region. The ions are then accelerated from the anode to cathode creating a 'focused'

beam. The resulted ion beam impinges upon a target material via a momentum transfer between an ion and target and sputters the material onto the substrate [15].

Ion beam sputtering technique possesses many advantages over other methods. Virtually all materials can be deposited since the coating material is passed into the vapor phase by mechanical rather than a chemical or thermal process. This makes it ideal for a variety of analytical techniques [16]. Ion beam sputtering is controllable due to low deposition rate when compared to other methods. This reduction in deposition rate allows thin films to be deposited uniformly onto the sample. Uniformity is of utmost importance in the neutron reflectometry experiments [17]. The above reasons make the ion beam sputtering to be a preferred method over others.

2.2 Neutron tunneling

Previously, a number of classical optics experiments were extended to neutron radiations such as slit diffractions, prism deflection, edge diffraction, diffraction on a ruled grating, interferometry experiments as well as various interferential based nanostructures such as multi-layered monochromators, polarizes and supermirrors [18-27]. The concept of tunneling and its experimental observation can be regarded as one of the early triumphs of quantum mechanics. The concept arises from quantum theory prediction that an initial state prepared in one classically allowed region of configuration space has a non-zero probability of penetrating through a classically forbidden region into a second classically allowed region [28].

The fundamental fact that every particle with mass is at the same time a wave was discovered in 1924 by de Broglie [29]. The optical behavior of light and neutrons is similar in many aspects yet the difference in the magnitude of the spin of photon and neutron brings about a certain distinction [30,31]. When light is incident on the interface of two media, it is partly transmitted into the second medium and partly reflected back into the first. If the refractive index of medium one is greater than that of medium two and the angle of incidence is larger than the critical angle, the total reflection occurs; the incident light is reflected completely back to medium one [32]. A fascinating phenomenon is the penetration of the wave, evanescent, into the second medium when the total reflection occurs. References to this work are contained in the paper by Hall [33], who reported in 1902 through experimental and theoretical investigations of the phenomenon. To investigate the

phenomenon experimentally, Hall chose the most common solution: the introduction of a third medium close to the first one. The second medium is now a thin film with a thickness of the order of the wavelength of light employed. The total reflection of light is thus "frustrated", a term coined by Leurgans and Turner in 1947 [34]. All three media are assumed to be transparent at the wavelength of operation. Hall examined the dependence of the penetration depth on the angle of incidence and polarization if the incident radiation for a different number of different media. He also represented a theoretical calculation for the transmission coefficient of the incident light. With regards to experimental verification of the relation between the transmission coefficient and the separation of the first media and the third media, Hall writes: "there seems, at present, no method for experimentally testing the theory for two media in the case of light waves. It would seem feasible, however, to test the theory with short electric waves". He was perhaps unaware that exactly such experiments had been performed by Bose as early as 1897. Bose examined the penetration of the waves by using the double prism arrangement [35]. Figure 2.2.1 is an example of the type of thin film Fabry-Perot resonator used by Hall.

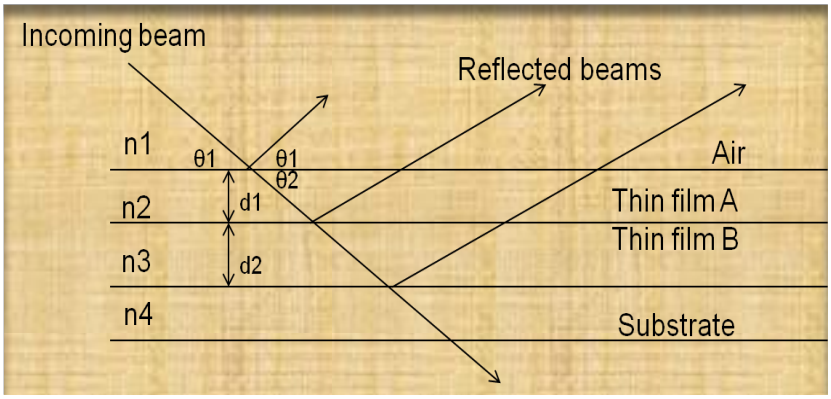

Figure 2.2.1: An example of the Fabry-Perot resonator that is used to observe this tunneling phenomenon.

The frustrated total reflection phenomenon was first observed in 1863 in classical optics by Quincke [36]. Quincke employed two prisms opposite each other while being separated by a thin film of air as the cavity. In the small wavelength range, the frustrated total reflection phenomenon was confirmed experimentally with X-rays by Croce and Pardo [37] using a Fabry-Perot cavity. In neutron optics, Steyerl and co-workers have also observed this tunneling phenomenon using Fabry-Perot cavities (resonators), but they only detected no more than two orders (first and second resonance orders). This was due to small available ultra-cold neutron intensity at the time [38-41].

This frustrated total reflection of neutron wave-particles shows itself by the existence of sharp dips in the plateau of total reflection due to resonant bound states in the nanostructured Fabry-Perot like-cavity [42]. The total reflection zone is characterized by the expected more or less dips due to tunneling resonances and the vitreous zone side is identified by the well-known Kiessig fringes interference pattern due to limited thickness of the different layers, from one medium to another, as shown in Figure 2.2.2 [43].

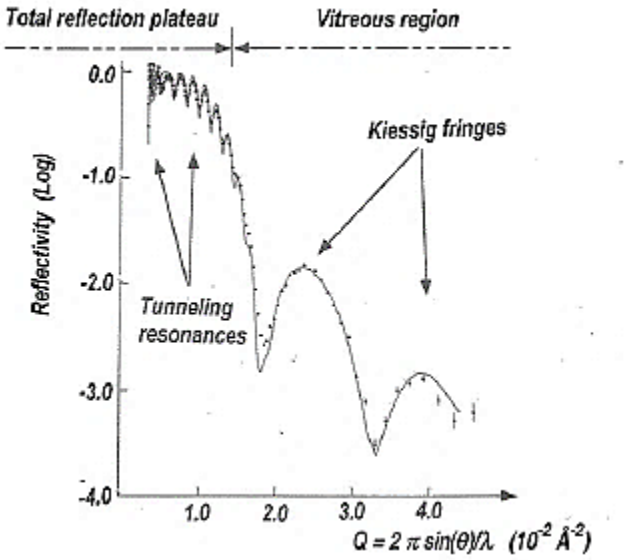

Figure 2.2.2: A graph showing how the tunneling phenomenon occurs [49].

The prerequisite to observe this phenomenon of frustrated total reflection, (the tunneling phenomenon), of neutron wave-particles suffering total reflection is the use of thin film Fabry-Perot resonators, also known as a Fabry-Perot cavity. The thin film Fabry-Perot resonator consists of transparent spacer material sandwiched between two highly reflecting mirrors. The transparent spacer layer must have a negative scattering length, as shown in Table 2.2.1, while the reflecting mirrors must have a positive scattering length, as shown in Table 2.2.2. The choice of thin film Fabry-Perot resonator is justified by the possibility to obtain numerous sufficiently sharp resonances and there's a small interdiffusion at medium interfaces [44]. A suitable material to

synthesize a Fabry-Perot resonator must be a high neutron reflector and have a small absorption scattering cross sections.

Table 2.2.1 Negative nuclear scattering length amplitudes (b_n) of some elements with low neutron absorption cross sections

element	**b_n(x 10^{-12}cm)**
Ti	-0.34
V	-0.05
Mn	-0.36
^{62}Ni	-0.87
^{152}Sm	-0.50

Table 2.2.2 Positive scattering lengths (b_n) of elements which are usually used as reflecting mirrors during synthesis of Fabry-Perot resonators.

Element	**b_n(x 10^{-12} cm)**
Ni	1.03
^{58}Ni	1.44
Fe	0.954
^{56}Fe	1.01

The frustrated total reflection, (the tunneling effect), of neutron wave-particles suffering the total reflection, was also observed with ultra-cold neutrons by Steyerl and co-workers [37]. The use of neutrons to observe frustrated total reflection is motivated by two reasons: The first is that the absorption in the use of neutrons is in a general manner very small and thus observation of the phenomenon in both reflection (resonant dips in the plateau of total reflection) and transmission (resonant peaks) is possible. The second is that the neutron possesses well-defined massive particle properties and thus the frustrated total reflection of neutron gives another manifestation

of tunneling effect and the proof of the wave-particle commentary principle of quantum mechanics [38].

There has been a lot of work documented on this kind of study in different systems, as shown in Table 2.2.3, different materials used for the synthesis of the Fabry-Perot resonator, using different radiations from cold neutrons, ultra-cold neutrons, and X-rays.

Table 2.2.3 some of the work that has been done in this tunneling phenomenon

System studied	Radiation nature	References
TiO_2-Ti-Si	Cold neutrons	[45]
Cu-Al-Cu	Ultra-cold and cold neutrons	[25]
SiO_2-PIQ-Si	X-rays	[46]
dPEP-PEP-dPEP	Cold neutrons	[47]
Ni-Al-Ni	X-rays	[48]
Ni-V-Ni	Cold neutrons	[49]

Since the frustrated total reflection, tunneling phenomenon, of neutron wave-particles suffering total reflection is observed in the Fabry-Perot cavities (resonators) it is important to know how neutrons propagate through these Fabry-Perot resonators. The interaction of an incident neutron plane wave at a grazing angle, usually less than 1^o, in different regions in the considered Fabry-Perot cavity is governed by a one dimensional Schrodinger equation given by :

$$\{ - \hbar / 2m\Delta_z + V(z)\}\Psi(z) = E(z)\Psi(z) \qquad (2.2.1)$$

where m is the neutron mass

$E(z) = \{hk(z)^2\}/2m$ is the incident-neutron energy in the z direction, k(z) is the component of the wave vector and V(z) is the optical potential that represents the effective interaction of the neutron with the system. In neutron optics, which is described as the behavior of waves interacting with matter, waves are characterized by their wavelength (frequency or momentum) while the matter is characterized by susceptibility, wave-matter interaction is characterized by the index of refraction from optical viewpoint [50]. So the neutron propagation in a Fabry-Perot cavity is also described by an effective refractive index:

$$n_j = 1 - \delta_j = \sqrt{1 - \xi_j / E} \qquad (2.2.2)$$

E is the neutron kinetic energy and ξ_j is the average Fermi pseudo potential of the cavity (resonator), whose expression is $\xi_j = 2\pi h^2 N_j b_j / m$. Where m, N_j, b_j *are* the neutron mass, the number of scattering nuclei per volume unit of medium j and its corresponding nuclear coherent scattering amplitude, respectively.

This phenomenon of frustrated total reflection observed with both cold and ultra-cold neutrons is of major importance as it could open new horizons in surface-interface investigations with neutron scattering techniques namely neutron reflectometry and neutron interferometry [35-38]. This phenomenon has enabled the performance of a continuing series of fundamental studies probing the properties of the neutron itself such as the neutron lifetime. As already established, this phenomenon exists through the manifestation of sharp dips, the widths of these dips are different: the lower the order the larger the width at half maximum. This is correlated to the neutron lifetime in the resonant cavity [35-38]. The values, of the width of dips, are more or less affected by both spectral and angular resolutions. Hence an accurate estimation of neutron lifetime requires a high collimation and high spectral resolution. It also reports some potential technological applications in neutron optics to make novel neutron optics devices such as monochromators, polarizers, and beam splitters. It also treats a peculiar phenomenon of Goos-Hanchen displacement, an optical phenomenon localized between the total reflection and the frustrated reflection extreme cases.

There is an application of Fabry-Perot configuration as neutron monochromators. The narrow bandwidth of monochromatic cold neutrons beams is of great value for a wide variety of scattering experiments. The way to obtain this type of beam by extraction from neutron guide tubes can be achieved by placing a monochromator inside the guide tube [51]. Another approach to producing high monochromatic beams could be the use of Fabry-Perot cavity under frustrated total reflection condition: The resonator could be placed in the neutron guide tube as one of the walls under the total reflection geometry, as depicted in Figure 2.2.3.

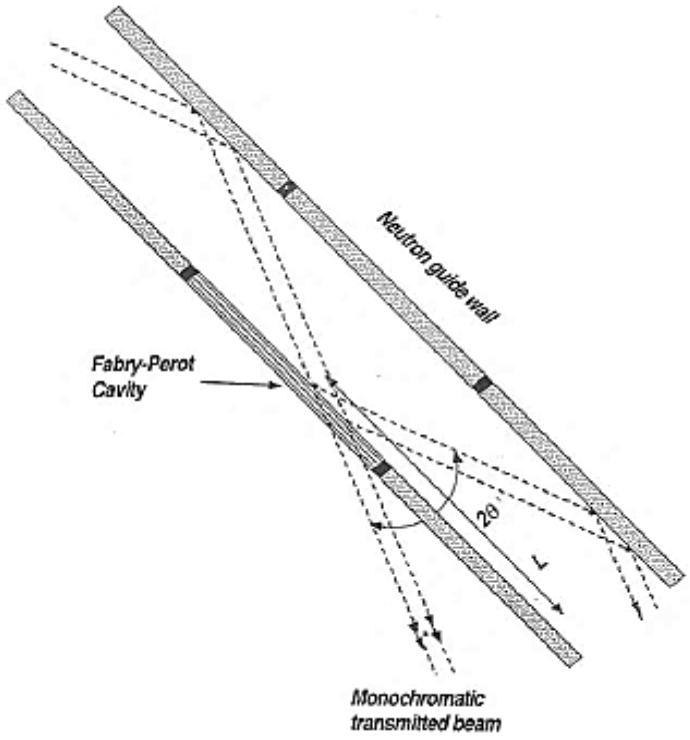

Figure 2.2.3: Shows as Fabry-Perot resonator placed inside the guide tube, as a monochromators. [49]

There are other applications for Fabry-Perot resonators. Its configuration is used as a neutron polarizer to produce polarized monochromatic cold neutron beams. The similar procedure used for the monochromator can be employed, however, the changing factor is the nature of layers of materials forming Fabry-Perot resonator while using the Zeeman Effect within the magnetic layers. Materials that are forming part of the Fabry-Perot resonators must present large coherent magnetic scattering amplitudes for one spin state to assure high polarization ratio [52]. Another potential application is the use of Fabry-Perot configuration as a neutron beam-splitter and neutron interferometry. The importance of neutron interferometry has been recognized over the years as it plays a key role in the quantum mechanics investigations concerning the neutron wave-particle duality [53-60]. There are three splitting methods that can be employed to split the beam: the perfect Bonse-Hart Silicon crystal [50-51], Ioffe diffraction grating systems [56] and the shearing geometry [61]. The first method allows a wide spatial beam separation within high intensity but is inapplicable for neutron wavelengths more than twice the Silicon crystal lattice parameter. The second one is interesting from neutron path inside the interferometer point of view as it is adapted

to cold neutrons but unfortunately it is limited in intensity. The third method very intense and coherent beams. The use of frustrated total reflection within the nano-structured Fabry-Perot cavities could be considered to split coherently intense neutron beams. In this configuration, there is, therefore, a spatial splitting by a tunneling phenomenon.

While the frustrated total reflection of neutron wave particles and different potential applications have been presented, it is important to mention a peculiar fundamental optical behavior of neutron wave packets suffering total reflection, the longitudinal Goos-Hanchen displacement. Similarities between neutron and the electromagnetic waves make observation of this phenomenon possible. The Goos-Hanchen longitudinal displacement was first predicted by Sir Isaac Newton as early as 1730 [62]. This phenomenon which is related to surface waves propagation has been observed for the first time by Herman Fritz Gustav Goos and Hilda Hanchen [63,64] in the optical visible spectral range. Since its observation, the longitudinal Goos-Hanchen displacement has triggered global interest [61]. Experimentally, this longitudinal Goos-Hanchen phenomenon, of totally reflected photon beams, is very significant as it allows achieving numerous studies including quantum mechanics. The possibility to observe this longitudinal displacement with totally reflected cold neutron beams is justified by low neutron absorption in general manner, optics similarity of neutron and electromagnetic waves, and grazing angle incidence. According to the Goos-Hanchen shift with photons and analogy between neutrons and photon optics, if the incident narrow and collimated monochromatic incident neutron beam impinges on the reflecting mirror, there will be longitudinal displacement of the reflected neutron beams. This phenomenon has been evaluated by various authors [65] [66-69]. Renard assumed that the cause of the shift is that for a finite incident plane wave suffering a total reflection, on average some energy enters into the medium of lower index (reflecting mirror) on one side of the beam and comes back into the medium of higher index (air) on the other side of the beam

References

[1] P. Moriarty, "Nanostructured materials.," *Rep.Prog.Phys.,* vol. 64, p. 297-381, 2001.

[2] S.N. Hari, "Nanostructured materials and nanotechnology;," London, Academic Press, 2002.

[3] G. Timp, "Nanotechnology," New York, Springer, 1999.

[4] R.P. Feynman, "Miniaturization," New York, Reinhold, p. 282-296,1961

[5] G.L. Stewart and K. a. M.M.Ward, "Benefits of combining top down and bottom-up," *Journal of nursing care quality,* vol. 30, no. 22, pp. 240-246.

[6] G.A. Obin and A.C.Arsenault, "Nanochemistry," RSC, 2005.

[7] P.M. Solomon, "Device innovation and material challenges at the limits of CMOS technology;," *Annu.Rev.Matter.Sci.,* vol. 30, p. 681, 2000.

[8] M.C. Nagel, "Frederick Soddy : from alchemy to isotopes;," *Journal of chemical education.,* vol. 59, no. 9, pp. 739-740.

[9] V.G. Plekhanov, "Isotopes in condensed matter," Heidelberg, Springer, p 3-293,2002

[10] V.G. Plekhanov, "Isotopic effects and disordering effect in long radius exciton spectroscopy," Moscow, p. 577-604,1997

[11] M. Toshiro, "Electronic properties of Nibium oxide thin films prepared by chemical vapor deposition," *Journal of electrochemical Society.,* vol. 141, no. 10, p. 2868.

[12] H. Windischman, "Intrinsic stress in sputter deposited thin films," *Rev.Sol.Mat.Sci.,* vol. 17, p. 54.

[13] J.D. Ferguson, G.Anikan, D.S.Dale, A.R.Woll and . J.D.Brock, "Measurement of surface diffusivity and coarsening during laser deposition,," *Physical Review Letters,* vol. 103, no. 25, p. 256103.

[14] K.S.S. Harsha, "Principles of physical vapor depostion of thin films," Great Britain, Elsevier, p. 400-410,2006

[15] P. D. Pochon, Ion beam deposition, oxford: MA Jones and Barlett Publishers, 2010.

[16] L.J. Bozzola, Electron Microscopy: Principles and Techniques for Biologists, Boston, 2000.

[17] F. Ott, A.Menelle and C. Fermon, "Neutron Reflectometry," vol. 70, 2009.

[18] C.G. Shull, *Phys.Rev.,* vol. 179, p. 752, 1969.

[19] H. Maier-Leibnitz and T.Springer, *Z.Phys.,* vol. 167, p. 386, 1962.

[20] F.J. Landkammer, *Z.Phys.,* vol. 189, p. 113, 1966.

[21] H. Kurtz H.Rauch, *Z.Phys.,* vol. 220, p. 419, 1969.

[22] H. Rauch and W.Treimer and U.Bonse, *Phys.Lett.,* vol. A47, p. 369, 1974.

[23] S.A.Werner, R.Collela and A.W.Overhauser and C.F.Eagen, *Phys.Rev.Lett.,* vol. 35, p. 1053, 1975.

[24] B.P. Schoeman D.L.D.Caspar and O.F.Kammer, *J.Apply.Cryst.,* vol. 7, p. 508-510, 1974.

[25] C.F. Majkrzack, *Physica(Utrecht),* vol. 136B, p. 69-74, 1986.

[26] F. Mezei and P.A. Dagleisch, *Commun.Phys.,* vol. 2, p. 41, 1977.

[27] J.B. Hayter and H.A.Mook, *J.Apply.Cryst.,* vol. 22, p. 35-41, 1989.

[28] A.Steyerl, T.Ebisawa and K. A.Steinbauser. Z.Utsuro, *Phys.,* vol. B41, no. 2, p. 283, 1981.

[29] K. Vladmir and V.Masahiko, in *Handbook of Neutron optics,* Wiley-VCH, 2010.

[30] V.F. Sears, "Neutron Optics", Oxford University Press, 1989.

[31] S.A. Werner and A.G.Klein, "Neutron Scatering," New York, Academic Press, 1986, pp. 303-318.

[32] M. Born and E.Wolf, "Principles of optics," Pergamon, Oxford, 1975.

[33] E. Hall, *Phys.Rev.,* vol. 15, p. 73, 1902.

[34] P.J. Leurgans and A.F.Turner, *J.Opt.Soc.Am,* vol. 37, p. 983, 1947.

[35] J.C. Bose, *Proc;R.Soc.London ser,* vol. A62, p. 300, 1897.

[36] G. Quincke, *An.Phys.Leipzig,* vol. 117, p. 1117, 1863.

[37] P. Croce and B.Pardo, *Nouv.Rev.Opt.Appl.,* vol. 4, no. 1, p. 229, 1970.

[38] V. K.Ignatovich, "The Physics of Ultra Cold Neutrons," Oxford-Clarendon Press, 1990.

[39] A. Steyerl, K.A.Steinhauser and S.S.Malik and H.Sheckenhofer, *Phys.Rev.Lett.,* vol. 44, p. 1306, 1980.

[40] A. Steyerl, T.Ebisawa , K.A.Steinhauser and M.Utsuro, *Z.Phys.,* vol. B41, p. 283-290, 1981.

[41] A. Steyerl, W.Drexel , S.S.Malik and E.Gutsmeidl, *Physica,* vol. B151, pp. 36-43, 1988.

[42] M. Maaza, L.P.Chernenko, D.A.Korneev, B.Pardo, C.Sella and F.Bridou, *Phys.Lett.,* vol. A218, p. 312-318, 1996.

[43] M. Maaza, B.Pardo, J.P.Chauvineau, F.Bridou, A.Menelle and A.Raynal and J.Corno, *Phys.Lett.,* vol. A235, p. 19-23, 1997.

[44] M. Maaza and B.Pardo and. F.Bridou, *Nucl.Instr.Meths.Phys.Res,* vol. A 326, pp. 531-537, 1993.

[45] Y.P. Feng, C.F.Majhrzrzal, S.K.Sinha, D.G.Wiesler, H.Zhang and H.W.Deman, *Phys.Rev.,* vol. B49, p. 10814, 1994.

[46] S.K. Sinha, M.Tolan, G.Vacca, Z.Li, M.Rafailovich, J.Sotolov, H.Lorenz, J.P.Kotthaus, Y.P.Feng , C.Gtiibel and D.Abernarthy, "On molecules in confined geometries," Proc.MRS Symp, 1995.

[47] L.J. Norton, E.J.Kramer, R.A.L.Jones, F.S.Bates, H.R.Brown and G.P.Fletcher and R.Kleb, *J.Phys.,* vol. 4, p. 367, 1994.

[48] P. Croce and B.Pardo, *Nouv.Rev.Opt.Appl.,* vol. 4, p. 229, 1970.

[49] M. Maaza, B.Pardo, J.P.Chauvineau, F.Bridou, A..Menelle, A.Raynal, *Z.Phys.,* 1996.

[50] T. Chupp, "Neutron optics and polarization," University of Michigan.

[51] B.P. Schoeman , D.L.D.Caspar and O.F.Kammerer, *J.Appl.Cryst.,* vol. 7, p. 508-510, 1974.

[52] M. Maaza and D.Hamidi, *Physics Reports,* vol. 514, p. 177-198, 2012.

[53] S.A. Werner, R.Collela and A.W.Overhauser and C.F.Eagen, *Phys.Rev.Lett.*, vol. 35, p. 1053, 1975.

[54] H. Rauch and W.Tremeir and U.Bonse, *Phys.Lett.A*, vol. 47, p. 369, 1974.

[55] A. Zeilinger, R.Gahler, C.G.Shull and W.Treimer and W.Mampe, *Rev.Modern Phys.*, vol. 60, no. 4, p. 1067, 1988.

[56] A.L. Frank, V.G.Nosov, *Phys.Atomic.Nuclei.*, vol. 57, p. 968, 1994.

[57] D.M. Greenberger and . A.W.Overhauser, *Rev.Modern Phys.*, vol. 51, p. 43, 1979.

[58] D.M. Greenberger, *Rev.Modern Phys.*, vol. 55, no. 4, p. 875, 1983.

[59] A. Ioffe, *Nucle.Instr.Meth.Phys.Res.A*, vol. 204, p. 565, 1983.

[60] H. Rauch, "Neutron Interferometry;," Oxford University Press, 1977, p. 162-193.

[61] M. Maaza, A.Menelle, M.Shamlal, B.Pardo and D.A.Korneev and L.P.Chernenko, *Phys.Lett.A*, vol. 195, 1994.

[62] S. I. Newton, "Optics," in *A Treateise of the Reflections, Refractions, Inflections and Colours of Light;*, London, 1730, p. 370.

[63] F. Goos and H.Hanchen, *Ann.Phys.*, vol. 6, no. 1, p. 333, 1947.

[64] F. Goos and H.Lindberg-Hanchen, *Ann.Phys.*, vol. 5, p. 251, 1949.

[65] J. Picht, *Z.Phys.*, vol. 30, p. 905, 1929.

[66] K. Artmann, *Ann.Phys.*, vol. 6, p. 87, 1948.

[67] C.V. Fragstein and C.Schaefer, *Ann.Physik.*, vol. 12, p. 84, 1953.

[68] J. Ricard, *Nouv.Rev.Opt.Appl.*, vol. 5, p. 7, 1974.

[69] R. J. *Nouv.Rev.d'Optique*, vol. 7, no. 1, p. 2, 1976.

Chapter 3

Neutron optics: background

Neutron optics is the branch of physics that deals with wave behavior of neutrons. The fact that every particle of mass is also a wave was discovered by de Broglie in 1925 [1]. He was honored for this discovery in 1929 by being awarded a Nobel Peace Prize in Physics.

This is de Broglie's fundamental formula:

$$\lambda = \frac{h}{p} \qquad (3.1)$$

λ is the distance between two consecutive peaks, which is the wavelength, h is the Planck's constant while p is the momentum.

DeBroglie's formula was experimentally verified by Davison and Thompson with the discovery of the diffraction of electrons [2,3]. A few months later, after their experiments, Kikuchi reported the characteristic pattern of electron diffraction and an important contribution which led to the establishment of quantum mechanics developed by Heisenberg [4]. The study of neutron optics began after the de Broglie's proof of matter waves following his Nobel lecture [5].

Neutron optics involves the study of the interaction of neutron beam with the matter. There are two ways in which free neutrons are sourced for neutron beams. One way is that neutrons are emitted in fission reactions at nuclear reactors. The other way is when neutrons are released in particle accelerator collision of proton beams with heavy targets of atoms such as tantalum. When neutrons are incident on a sample of matter the neutrons can be reflected, scattered, transmitted, or diffracted depending on the composition and structure of the sample material [6]. The types of neutrons employed in probing matter are slow neutrons because unlike fast neutrons, they have longer wavelengths of about 10^{-10} meters which makes them show the wave-like behavior when interacting with matter. Slow neutrons that are scattered by atoms in the matter undergo interference, just like x-rays and light, to form a diffraction pattern that contains details such as crystal structure and magnetic properties of the matter [7].

Since the discovery of neutrons 85 years ago [8], they have been recognized as the tool for probing atomic nucleus. It was Fermi, in 1934, who discovered the effectiveness of slow neutrons during the experiment on artificial radioactivity. Elsasser, 1936, first suggested that if the neutrons are governed by quantum mechanics, then they should be diffracted by crystalline materials. Those properties were later confirmed by diffraction experiments from crystals by Halban and Preiswerk, 1936, as well as Mitchell and Powers [9], which exhibited that thermal neutrons behave accordingly with de Broglie's hypothesis and had a wavelength comparable with x-rays. The analogy between x-ray scattering and neutron scattering reflects the behavior of waves of comparable wavelength, although the nature of individual interaction varies. In the case of x-rays, the interaction is electromagnetic while in the case of neutrons it is nuclear interaction [10].

In the early experiments, neutrons came from nuclear reaction responsible for their discovery, namely $^{9}Be\ (\alpha, n)^{12}\ C$. Thus, a radioactive alpha sources such as polonium were mixed with powdered beryllium and neutrons were thermalized in hydrogen moderators. With the help of fission reactors providing more flux of neutrons, beams became available. At the same time, beams of thermal neutrons became known and established as significant in probing of structure condensed matter. The behavior of thermal neutrons as seen in Bragg diffraction was an early verification of quantum mechanical principles [11]. This was made possible by properties of neutrons such as mass, lack of electric charge, which makes neutron penetrate deep into the matter. These properties have made it possible to probe certain aspects of quantum mechanics which has remained unexplored. The example of the above statement would be the observability of relative phase shifts by means of neutron interferometry [12]. Also during the early experiments, slow neutrons have been shown to exhibit the Bragg diffraction as well as many phenomena of classical optics such as refraction [13]. In the past decade, many experimental efforts have been in place to study the neutrons with kinetic energies of about 10^{-7} eV, which is five orders and more of magnitude lower than the energy of thermal neutrons [14]. The reason of interest in ultracold neutrons is because their energies are smaller than the mean potential in material, $E > V$. This means that total reflection will occur for all angles of incidence. This fact makes it easier for ultracold neutrons to be confined in closed materials cavities or bottles as this was proposed by Zeldovich in 1959 [15].

In principle, it should be possible to store neutrons in closed containers for about 12 minute, which is its natural lifetime. However, in practice it has been shown that confinement times decreases by one to two magnitude of orders, this can be accounted by inelastic scattering from surface impurities.

3.1 Neutron refractive index approximation

Theory of reflection takes into consideration an ideal situation where neutron wave is impinging onto planar surface separating the vacuum and homogenous medium characterized by potential and refraction index describing neutron interaction with reflecting layers.

As in any bulk system, the neutron-atom interaction is described via the Fermi potential:

$$v(r) = \frac{2\pi h^2}{m} b\delta(r) \qquad (3.2)$$

Where r is the distance from the neutron to the nucleus, m is the neutron mass, b is the scattering length and h is the Planck's constant.

The wavelength of neutron wave-particles is larger than interatomic distances in the matter this makes the waves to interact with many nuclei [16]. Since the neutron wave particles interact with nuclei, their interaction is defined as:

$$\nabla = \frac{2\pi h^2}{m} \mathrm{N}b \qquad (3.3)$$

$\mathrm{N}b$ is constant in the film and it's a scattering length density (SLD), N is the number density and b is the scattering length of the elements making up the thin film [17]. Neutron needs to have a kinetic energy in order to propagate from vacuum to the inside of the medium. In a vacuum, the neutron has a kinetic energy of:

$$\mathrm{E} = \frac{h^2 \kappa_o^{\,2}}{2m} \qquad (3.4)$$

Once the neutron is inside the medium, its kinetic energy is as follows:

$$\mathrm{E} = \frac{h^2 \kappa^2}{2m} + \nabla \qquad (3.5)$$

When taking conversation of energy into consideration, it gives:

$$\frac{h^2\kappa_o^{\ 2}}{2m} = \frac{h^2\kappa^2}{2m} + \nabla = \frac{h^2\kappa^2}{2m} + \frac{2\pi h^2}{m}\mathrm{N}b \ (\text{since}\ \nabla = \frac{2\pi h^2}{m}\mathrm{N}b) \quad (3.6)$$

which translates in terms of momentum into the following:

$$\kappa_0^{\ 2} - \kappa^2 = 4\pi \mathrm{N}b \quad (3.7)$$

Since $\frac{\kappa}{\kappa_o} = n$ which is the refractive index by definition and $\mathrm{N}b$ is small in the order of about (10^{-6} A^{-2}), the following equation, which is the refractive index for neutrons [18], is obtained:

$$\mathrm{n} = 1 - \lambda^2 \mathrm{N}b / 2\pi \quad (3.8)$$

Neutron has quite a number of properties. The currently known properties and their values are shown in Table 3.1 [19]

Table 3.1 Fundamental properties of neutrons

Property	**Value**
Mass : m	1.6747×10^{-24}g
Spin : s	$1/2$
Charge : q_n	$< -1.5 +/- 1.4 \times 10^{-20}$ e
Magnetic dipole moment : u_n	6.032×10^{-12} e VG^{-1}
Life-time : t_n	937 +/- 18 s
Electric-dipole moment	$< 10^{-24}$ e cm
g factor: g_n	-1.913
Gyromagnetic ratio : $\gamma = \frac{2u_n}{h}$	1.833×10^4 $s^{-1}G^{-1}$

Due to neutron's magnetic dipole –moment, a neutron in a magnetic field B has an interaction potential:

$$V_{mag} = - u_n .B = \pm u_n B \qquad (3.9)$$

The $\pm$ sign corresponds to parallel or anti-parallel of neutron spin to the direction of the field. The refractive index for the ferromagnetic material is:

$$n^2 = 1 - \frac{\lambda^2 N}{\pi}(b \pm \rho) \qquad (3.10)$$

where p is regarded as the magnetic scattering length. This exhibits the two different spin states of neutron follow different trajectories. The two-valued nature of refractive index for ferromagnetic materials makes them to be birefringent and gives a basis for experiment with polarized neutrons [20].

3.2 Reflection

In the definition of neutron optics, it is mentioned that neutrons can be either reflected, scattered and diffracted. The mirror reflection of neutrons was first observed by Fermi and Zinn [21-23] on July 14, 1944, using collimated beam from a thermal column of the CP3 reactor at the Argonne National Laboratory. The further studies by Fermi and Marshal (1947) were among the earliest verifications of neutron optics. They measured the critical angle for different surfaces using neutrons monochromated by Bragg scattering and they also established a significant way of determining scattering length [18]. In another experiment by Hughes and Burgy in 1951, they used neutron beam filtered through polycrystalline beryllium oxide. These filters would allow passage of all neutrons whose wavelengths exceed the Bragg limitations. Due to the wavelength spread of the filtered beam, the critical angle is less sharply defined, which then limits the accuracy of refractive index measurements, However, accuracies approaching 0.2% are attainable in measurements which compare one scattering length with another [24]. Other investigators have used the technique to measure the refractive index of solid surfaces, including thin films [25]. In all these experiments, the high accuracy is limited by wavelength and its distribution. However, the limitation is avoidable by the technique of gravity refractometer came with Maier-Leibnitz in 1962 [26]. In this technique it is observed that the mean potential energy of neutrons in the matter is comparable in magnitude to the energy acquires by neutrons when falling through a gravitational potential difference: *mgh*, where the height of fall, h, is the order of 1 m. This means that the falling

neutrons in a horizontal beam cannot penetrate a horizontal plane surface they have fallen through a minimum height, h_o,

$$mgh_o = \nabla = \frac{2\pi h^2}{m} Nb \qquad (3.11)$$

If the height of fall exceeds h_o which is in the order of 1 m, then neutrons will penetrate the mirror otherwise they will be totally reflected. h is a measure of Nb and hence of scattering length b [10]. In previous years, all the classical optical phenomena that can be produced with x-rays have also been demonstrated with neutrons leading to the construction of neutron optical instruments that produces significant tools for studies in physics, chemistry, and biology [6]. The reflection of neutrons is due to the real part of the index of refraction and reflectivity measurements allow the direct determination of both the sign and magnitude of the coherent scattering length [27-30]. This technique is employed in the neutron gravity refractometer [31] [32] which has led to the accurate determination of coherent scattering length, b , for many elements [33]. The total reflection of thermal neutrons at grazing angle incidence is used for the construction of guide tubes for transport of neutron beams [34,35], while the reflection of cold neutrons is used for the construction of neutron bottles [36,37].

3.3 Transmission

When neutrons interact with matter can also be transmitted. In the transmission of neutrons, the decrease in intensity of neutron beams traversing matter is thought of from a particle viewpoint as it is due to absorption and scattering of neutrons by atoms in the matter (sample), which is determined by total collision cross section [10]. Transmission can also be thought from wave viewpoint as it is due to quantum mechanical interference between the incident wave and scattered wave. Transmission is determined by the imaginary part of the index of refraction. The measurements of transmission also lead to the determination of coherent scattering length [28].

3.4 Refraction

Neutron beams can also be refracted, the refractive bending of neutron beams also gives an accurate method of determining scattering lengths [38-40] . The variation of the angle of deflection with neutron wavelengths allows manufacturing of monochromators for ultracold neutrons [41-

43] . A refractive lens in these devices is used for focusing the beam. Usage of shaped magnetic fields for bending and polarizing neutron beams has also been revealed [44]. The geometrical theory of optics assures that the potential V(r) changes slowly from point to point in space. This is not the case for the interaction of slow neutrons with the matter because the spacing between nuclei is a few angstroms, and comparable to neutron's de Broglie wavelength. In 1934 Fermi concluded that in complete comparison with the refraction of light (x-rays), the interaction of neutrons with materials consists of coherent scattering. In bulk non-magnetic material (matter) the scattering is mainly by the atomic nuclei for which the interaction is strong and short-range [45]. For all nuclei interaction the potential is attractive and can be denoted by a potential well of depth $-V_o$ (10 – 60 MeV) and radius R (of order 10^{-12} cm) as depicted in Figure 3.1. The interaction of neutrons with the material can be characterized by an index of refraction:

$$n(r) = \mathrm{K}(r) \Big/ \kappa \tag{3.12}$$

The propagation constant, wave vector *k*, in free space is given by:

$$\kappa = \sqrt{2m\mathrm{E}} \Big/ h \tag{3.13}$$

Materials with an index of refraction which is less than 1 are externally reflected by neutrons. This is why many materials are made into mirrors to reflect neutrons.

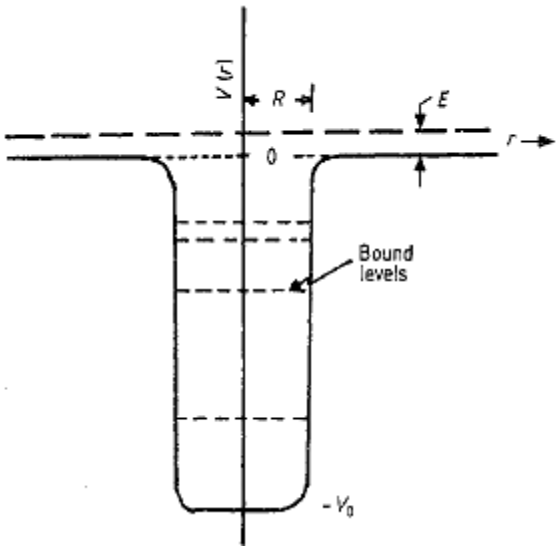

Figure 3.1. The attractive neutron nuclear potential well. E is the kinetic energy of neutron.

Neutron wave particles behave differently under different conditions. The two other effects are Fraunhofer and Fresnel diffraction. Fraunhofer is the most widely used neutron optical effect by crystal lattices (Bragg reflection). Bragg reflection can be used for crystal structure and magnetic structure determination [46,47]. The observed Bragg reflection in large crystals exhibit number of unique effects including anomalous absorption [48,49] and Pendellosung interference [50] [51,52]. Pendellosung interference provides an accurate method for scattering length determination. The Bragg reflection by large crystals is also a method for the production of monoenergetic neutron beams and for the energy analysis scattered by the neutrons [53]. Furthermore, Bragg reflection can be used in the study of structural and magnetic inhomogeneity in the crystal by means of neutron topography [54-57]. Small-Angle Scattering of neutrons (SANS) is another example of Fraunhofer diffraction effect with numerous applications in physics, chemistry, and biology [58].

There's a difference between Fraunhofer and Fresnel diffraction. The difference is in the conditions of the experiment. In Fraunhofer diffraction, the source and the detector are both at infinity and diffraction patterns depend only on the angles of scattering. Whereas on Fresnel the diffraction pattern depends only on the finite value of the distance from the diffracting element to the source or the detector. Therefore, Fraunhofer diffraction can be described in terms of differential scattering cross section while Fresnel diffraction cannot. The Fresnel diffraction of neutrons by ferromagnetic domain boundary has been shown [59-60]. A concave reflecting Fresnel zone mirror and Fresnel plate [36] have been used to focus beam with ultracold neutrons.

These neutron optical phenomena listed above all have one thing in common, that is they all arise from coherent elastic scattering. The fundamental quantity of neutron optics is a coherent wave Ψ , which provides a description of the coherent elastic process and satisfies the Schrodinger equation:

$$\{ - \hbar/2m \, \Delta + \nu(r)\}\Psi(r) = E\Psi(r) \} \qquad (3.14)$$

In which v(r) is the optical potential, E is the incident neutron energy and m is the mass of the neutron. In neutron optics, all collision processes other than coherent elastic scattering are called absorption. Absorption does not only mean the absorption of a neutron by nuclei but also diffuse scattering, which is incoherent scattering.

3.5 Theory of optics

The theory of optics is divided into two parts: The theory of dispersion and the theory of reflection, refraction, and diffraction, which has been already discussed. The theory of dispersion is concerned with deriving Schrodinger equation [61-64]. This theory is concerned with the proof of Schrodinger equation. Theory of reflection, refraction, and diffraction is concerned with the solution of Schrodinger equation. The theory of dispersion has two different stages: The first stage is the proof that the coherent wave ψ (r) satisfies Schrodinger equation and the second stage deals with the derivation for the potential optical potential ν (r) [65]. The first stage can be conducted generally while for the second stage it is necessary to be specific about the nature of the interaction between neutrons and the matter in terms of how atoms are in the matter. Whether atoms are held at fixed positions or free, whether the matter is monoatomic or polyatomic. For the derivation of optical potential, it is best to stick to simple matter systems such as monoatomic since such matter system is non-magnetic in order to avoid unnecessary complexities. During this derivation, the interaction between neutron and nuclei is taken into account. It was then found that in first approximation [40], that the optical potential is given by the equilibrium value of Fermi pseudo-potential:

$$\nu(r) = \frac{2\pi\hbar^2}{m} pb \qquad (3.15)$$

3.6 Ferromagnetic mirrors as neutron polarizers

Ferromagnetic mirrors can be used as neutron polarizers; the technique of producing polarized neutron beams came from the experiment of Hughes and Burgy [66], who were the first to explore the reflection of neutrons from magnetized mirrors. The use of big ferromagnets as polarizing mirrors had difficulties because a large size required by a small value of critical angle and large magnets requires saturating the mirror material. The solution to this is to employ thin evaporated films of ferromagnetic alloys [67] deposited on index material substrates. These thin films were able to be magnetized by small magnets. The interface magnetizations of ferromagnetic transition metal in Fe-SiO and Ni-O multi-layered films have been studied by Sato *et al* [68] using small angle scattering neutron technique. In that experiment, Fe showed no reduction of the interface

magnetization while Ni had a large reduction of magnetic moment at interfaces which indicated the possibility of a magnetic dead layer.

References

[1] L. deBroglie, "Recherches Sur La Theorie des quanta," *Atm.des Phys.10eser,* vol. 3, p. 22-28, 1925.

[2] L. C. Davisson, "Diffraction of electrons by a crystal nickel," *Phys.Rev.,* vol. 30, p. 705-740, 1927.

[3] G. Thomson and A.Reid, "Diffraction of cathode rays by a thin film," *Nature,* vol. 119, p. 890, 1927.

[4] W. Heiserberg, "Die Physikalischen Principlen der Quanten theorie," *Varlag von,* 1930.

[5] L. deBroglie, "The wave nature of electron," *Nobel Lecture, The Nobel Foundation,* 1929.

[6] V.F. Sears, "Physics Reports," vol. 1, no. 82, p. 1-29, 1982.

[7] R. Gahler, A.G.Klein and A.Zeilinger, *Phys.Rev,* vol. A23, p. 164-167, 1981.

[8] J. Chadwick, "Possible existence of a neutron," *Proc.Roy.Soc,* vol. 130, p. 692-708, 1932.

[9] D.P. Mitchell and P.N.Powers, "Bragg reflections of slow neutrons," *Phys.Rev,* vol. 50, no. 5, p. 486-487, 1936.

[10] A.G. Kelin and A.Zeilinger, *Phys.Rev,* vol. 23, p. 164-167, 1981.

[11] P.K. Iyengar, "Thermal neutron scattering," New York, New York : Academic, 1965, p. 98-138.

[12] S. Kikuta, "Neutron interferometry," Oxford University Press, 1979, p. 60-75.

[13] D. Hughes, "Neutron optics," New York, New York : Wiley Interscience, 1954.

[14] G.L. Squires, "Introduction to theory of Thermal Neutron Scattering," Cambridge : Cambridge University Press, 1978.

[15] Y.U. Zeldovich, *Sov.Phys.,* vol. 9, p. 1390, 1959.

[16] R. H, "Neutron Matter Wave Quantum Optics," *Found Phys,* vol. 42, p. 760-762, 2012.

[17] J.C. Lauter, "Polymer Science," Elsevier, p. 411-433,2012

[18] R.Pynn, "Neutron Reflectometry," Indiana University and Spallation Neutron Source.

[19] G. J. Byrne, *Phys. Lett.,* vol. 92B, pp. 274-8, 1980.

[20] J.B.Hayter, "Neutron Diffraction," Berlin, Springer-Verlag, 1978, pp. 41-70.

[21] E. Fermi, "Collected papers," vol. 217, University Chicago Press, p. paper no.217,1962.

[22] E. Fermi and W.H.Zinn, *Phys.Rev,* vol. 70, p. 103, 1946.

[23] E. Fermi and W.H.Zinn, in *Cambridge Conference , paper 220*, 1947.

[24] D.J. Hughes and M.T.Burgy, *Phys.Rev.,* vol. 81, p. 498, 1951.

[25] D. Bally, S.Todiranus, S.Rippeanu and M.G.Bellon, *Rev.Sci.Instrum.,* vol. 33, p. 916, 1962.

[26] H. Maier-Leibnitz, *Z.Angew.Phys.,* vol. 14, p. 438, 1962.

[27] D.J. Hughes, "Neutron optics," Interscience, New York, 1954.

[28] G.E. Bacon, "Neutron diffraction," Claredon Press, Oxford, 1975.

[29] E. Fermi and L.Marshall, *Phys.Rev.,* vol. 71, p. 666, 1947.

[30] T.A. Kitches and T.Oversluizen and L.Pasell, *Phys.Rev.Lett,* vol. 32, p. 791, 1947.

[31] Maier-Leibitz, *Z.Angew.Phys.,* vol. 14, p. 738, 1962.

[32] L. Koester, *Phys.*, vol. 152, p. 328, 1965.

[33] L. Koester and R. S. L. T. d. quanta, "Recherches Sur La Theorie des quanta," *Atm.des Phys.*, vol. 10, p. 1, 1965.

[34] J. Christ and T.Springer, *Nukleonik,* vol. 4, p. 23, 1962.

[35] H.Maier-Leibnitz and T.Springer, "Neutron Physics," *J.Nucle.Energy,* vol. 17, p. 217, 1963.

[36] A. Steyerl, "Neutron Physics," *Springer Tracts in Modern Physics,* vol. 80, p. 57-130, 1977.

[37] R. Golub and J.M.Pendlebury, *Rep.Prog.Phys.*, vol. 42, p. 439, 1979.

[38] C.S. Schneider and C.G.Shull, *Phys.Rev.B,* vol. 3, p. 830, 1971.

[39] C.S. Schneider, *Rev.Sci.Instrum.*, vol. 44, p. 1594, 1973.

[40] C.S. Schneider, *Act.Cryst.*, vol. A32, p. 375, 1976.

[41] P.D. Kearney, A.G.Klein and G.I.Opat and P.Dahler, *Nature*, vol. 257, p. 313, 1980.

[42] R. Gahler and J.Kalus and W.Mampe, *J.Phys.Rev.*, vol. E13, p. 546, 1980.

[43] R. Gahler and A.G.Klein and A.Zeilinger, *Phys.Rev.*, vol. A23, p. 546, 1981.

[44] W. Just, C.S.Schneider and R.Coscweski and C.G.Shull, *Phys.Rev.*, vol. B7, p. 4142, 1973.

[45] E. Fermi, *m Nuovo Cim.*, vol. 11, p. 157, 1934.

[46] H. Dachs, "Neutron Diffraction," Berlin, Springer, 1978.

[47] G.E. Bacon, "Neutron Diffraction," Clarendon Press ,OXford, 1975.

[48] J.W.Knowles, *Acta.Cryst.*, vol. 9, p. 61, 1956.

[49] D. Sippel and K. a. G.E.R.Schulze, *Phys.Lett.*, vol. 8, p. 241, 1964.

[50] C.G. Shull, *Phys.Rev.Lett.*, vol. 21, p. 1585, 1968.

[51] C.G. Shull and J.A.Oberteuffer, *Phys.Rev.Lett.*, vol. 29, p. 871, 1964.

[52] C.G. Shull and W.M.Shaw, *Z.Naturforsch*, vol. 28a, p. 657, 1973.

[53] P.K. Iyengar, "Thermal neutron scattering;," New York, Academic Press, 1965, p. 97.

[54] K. Doi, N.Minakawa and H. a. N.Masaki, *J.Apply.Cryst.*, vol. 4, p. 528, 1971.

[55] M. Ando and S.Hosoya, *Phys.Rev.Lett.*, vol. 29, p. 28, 1972.

[56] M. Schlenker and C.G.Shull, *J.Appl.Phys.*, vol. 44, p. 481, 1978.

[57] M. Schlenker and J.Baruchel, *J.Apply.Cryst.*, vol. 49, p. 1996, 1978.

[58] W. Schmatz and T.Springer and J.Schelter, *J.Appl.Cryst.*, vol. 7, p. 96, 1974.

[59] G. Schutz and A.Steyerl and W.Mampe, *Phys.Rev.Lett.*, vol. 44, p. 14, 1980.

[60] A.G. Klein and G.I.Opat, *Phys.Rev.Lett.*, vol. 37, p. 238, 1976.

[61] H.A. Lorentz, "The theory of electrons," New York, Dover, 1952.

[62] P. Mazur and B.R.A.Njboer, *Physica.*, vol. 19, p. 971, 1953.

[63] P. Mazur, *Adv.Chem.Phys.*, vol. 1, p. 309, 1958.

[64] J. Van Kranenskon and J.E.Sipe, *Prog.Opt.*, vol. 15, p. 245, 1977.

[65] V.F. Sears, *J.Phys.*, vol. 56, p. 1261, 1978.

[66] D.J. Hughes and M.T.Burgy, *Phys.Rev.*, vol. 81, p. 498-506, 1951.

[67] B. Hamelin, *Nucl.Instrum.Meth.*, vol. 135, p. 299-306, 1976.

[68] M. Sato, K.Abe, Y.Endoh and J.Hayter, *J.Physc:solid.Phys.*, vol. 13, p. 3563-76.

Chapter 4

Data modeling and Simulation

4.1 Modeling

Modeling is the process of producing a model [1]. A model is the representation of the working system. It is similar but simpler than the system it is representing and it has to be defined by parameterizing it to reflect the details of the study. The purpose of the model is to predict the effect of changes to the system [2]. Using a model to investigate systems or phenomena is less laborious and more flexible than direct experimentation. There are many reasons why investigations cannot be carried by direct experimentation. The experiment can be disruptive or be dangerous. An important issue in modeling is the validity, model validation includes simulating the model under known input conditions and comparing model output with system output [3].

4.2 Simulation

The words simulation and modeling are used interchangeably in some context due to their blended role. A model provides the basis for the simulation to create an image of a real system or phenomena. Simulation refers to the application of computational models to study and predict the physical events [4]. Computer simulations represent an extension of theoretical science in that it is based on mathematical models and those models attempt to characterize the physical predictions of scientific theories. A simulation can also take the form of a computer-graphics image that represents the dynamic process in an animated sequence [4]. Simulation can be used to explore new theories and also design new experiments to test those theories. It also provides an alternative when phenomena are not observable or expensive [5].

4.3 How to select simulation software

A simulation model can be built using general purpose programming languages which are familiar to an analyst. However, nowadays simulation studies are implemented using simulation package. The advantages include reduced programming requirements for communication. The question of how to select best simulation software lies in the ease of use, code re-usability, graphic user interface, hardware and software requirements, output reports and graphical plots. There are two types of simulation package. The language and application-oriented simulator. Language simulation package requires varying amount of programming expertise while the application-

oriented simulator is easier to learn even for less experienced users who don't have strong programming background [6].

In this study Program Reflex13 software is employed to simulate specular reflectivity data. The quantity that is measured is the reflectivity, R, as the function of the momentum wave vector transfer, which is defined as follows:

$$Q = 4\pi \sin \theta / \lambda \qquad (4.1)$$

where λ is the neutron wavelength and θ is the angle of incidence.

The measured reflectivity, R(Q), results from the specular reflections originated by changes in the refractive index in the material in a perpendicular direction to the reflecting surface.

4.4 Program Reflex13

Program Reflex13 is a Matlab routine for simulation of specular X-ray and neutron reflectivity data with the matrix technique [7]. The program is still in its developmental stage, so no information is available in the literature about it except lecture notes [8] which briefly described the matrix technique which is employed by this Program Reflex13. This means that some features such as save and fit are not fully operational as this program is still a work in progress.

4.4.1 Matrix technique

In explaining the matrix technique, a polarized wave in the direction perpendicular to the plane of the incidence propagating into a stratified medium is considered. The axes are chosen so that the wave is traveling in the *x*0*z* plane as shown in Figure 4.1. The air is labeled as medium 0 and strata or layers with different scattering length densities are identified by $1 \leq j \leq n$ downwards. In the notation, the depth Z_{j+1} marks the interface between j and j+1 layers. The wave traveling through a material is transmitted and reflected at each interface and the amplitudes of the upwards and downwards traveling waves are defined as A^-+ and A^+ respectively. The electric field E^- of the downwards wave traveling wave in the jth stratum is given by the solution of the Helmholtz equation:

$$\mathrm{E}^{-} = \mathrm{A}^{-} e^{+i(\omega t - k_{inx,jx} - k_{inz,jz})} \hat{e}y \qquad (4.2)$$

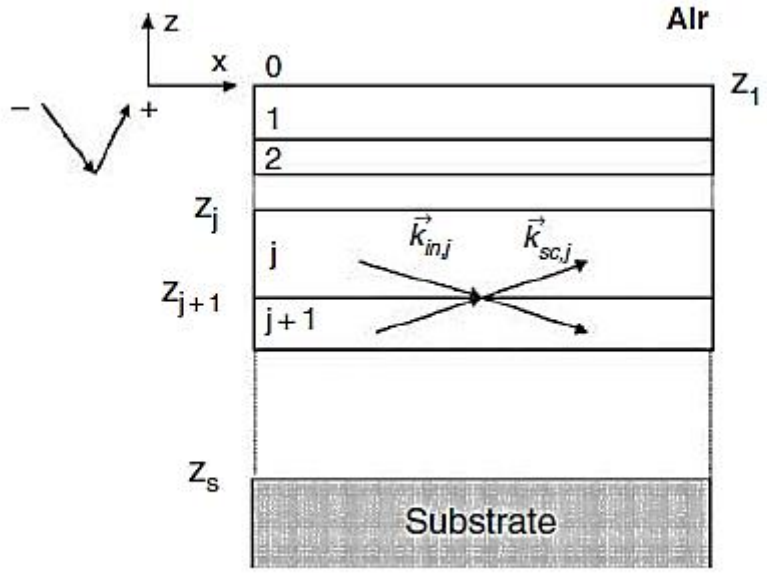

Figure 4.1: Illustration of the plane of incidence for a stratified medium. The signs label the direction of propagation of the wave, air is medium 0 and strata are identified by $1 \leq j \leq n$ layers in which upwards and downwards waves travel.

The following notation is adopted in the derivation:

$$k_{inx,j} = k_j \cos\theta_j$$

$$k_{inz,j} = -k_j \sin\theta_j = -\sqrt{k^2{}_j - k^2{}_{inx,j}} \qquad (4.3)$$

The value of $k_{inx,j}$ is conserved at each interface since the condition is imposed by the Snell-Descartes' law of refraction. The upward and downward waves traveling waves are superimposed at each interface so that at depth z from the surface the electric field in medium j is:

$$\mathrm{E}_j(x,z) = (\mathrm{A}_j^{+} e^{ik_{inz,jz}} + \mathrm{A}_j^{-} e^{-ik_{inz,jz}})\, e^{+i(\omega t - k_{inx,jx})} \qquad (4.4)$$

As $k_{inz,j}$ takes a complex value, the magnitude of the upwards and downwards electric field in layer j is denoted by

$$U(\pm k_{inz,j,z}) = \mathrm{A}_j^{\pm}\, e^{\pm i k_{inz,jz}} \tag{4.5}$$

In addition, the quantity $k_{inz,j}$ is replaced by $k_{z,j}$. The condition of continuity of the tangential component of the electric field and the conservation of $k_{x,j}$ at the depth Z_{j+1} of the interface j , j+1, lead to

$$U(k_{z,j}, Z_{j+1}) + U(-k_{z,j}, Z_{j+1}) = U(k_{z,j+1}, Z_{j+1}) + U(-k_{z,j+1}, Z_{j+1}) \tag{4.6}$$

The tangential component of the magnetic field is continuous when the derivative of the electric field is conserved. This leads to the equality below at j, j+1 interface

$$k_{z,j}[U(k_{z,j}, Z_{J+1})] = k_{z,j+1}[U(k_{z,j+1}, Z_{j+1}) - U(-k_{z,j+1}, Z_{j+1})] \tag{4.7}$$

The combination of these two equations can be written in a matrix form so that the magnitudes of the electric field in media j, j+1 at depth Z_{j+1} must satisfy:

$$\begin{bmatrix} U(k_{z,j}, Z_{j+1}) \\ U(-k_{z,j}, Z_{j+1}) \end{bmatrix} = \begin{bmatrix} P_{j,j+1}, m_{j,j+1} \\ m_{j,j+1}, p_{j,j+1} \end{bmatrix} \begin{bmatrix} U(k_{z,j+1}, Z_{j+1}) \\ U(-k_{z,j+1}, Z_{j+1}) \end{bmatrix} \tag{4.8}$$

With

$$P_{j,j+1} = \frac{k_{z,j} + k_{z,j+1}}{2k_{z,j}}$$

$$m_{j,j+1} = \frac{k_{z,j} - k_{z,j+1}}{2k_{z,j}} \tag{4.9}$$

The matrix which transforms the magnitude of the electric field from medium j to the medium j+1 is called refraction matrix $\Re_{j,j+1}$. In addition, the amplitude of the electric field within the medium j varies with depth as follows:

$$\begin{bmatrix} U(k_{z,j}, Z) \\ U(-k_{z,j}, Z) \end{bmatrix} = \begin{bmatrix} e^{-ik_{z,j}h} & 0 \\ 0 & e^{ik_{z,j}h} \end{bmatrix} \begin{bmatrix} U(k_{z,j}, Z+h) \\ U(-k_{z,j}, Z+h) \end{bmatrix} \tag{4.10}$$

The matrix which is involved is denoted by the translation matrix $\Im$. The amplitude of the electric field at the surface (depth Z = 0) of the layered material in figure 4.1 is obtained by multiplying all the refraction and translation matrices in each layer starting from substrate (at z = Z_s) as follows

$$\begin{bmatrix} U(k_{z,0}, Z_1) \\ U(-k_{z,0}, Z_1) \end{bmatrix} = \Re_{0,1}\Im_1\Re_{1,2}\ldots\Re_{N,s}\begin{bmatrix} U(k_{z,s}, Z_s) \\ U(-k_{z,s}, Z_s) \end{bmatrix} \quad (4.11)$$

All the matrices in the above product are 2x2 matrices so that their product which is called the transfer matrix m is also a 2x2 matrix. We therefore have,

$$\begin{bmatrix} U(k_{z,0}, Z_1) \\ U(-k_{z,0}, Z_1) \end{bmatrix} = m \begin{bmatrix} U(k_{z,s}, Z_s) \\ U(-k_{z,s}, Z_s) \end{bmatrix} \begin{bmatrix} M_{11} & M_{12} \\ M_{21} & M_{22} \end{bmatrix} \begin{bmatrix} U(k_{z,s}, Z_s) \\ U(-k_{z,s}, Z_s) \end{bmatrix} \quad (4.12)$$

The reflection coefficient is defined as the ratio of reflected electric field to incident electric field at the surface of the material and is given by

$$r = \frac{U(k_{z,0,}Z_1)}{U(-k_{z,0,}Z_1)} = \frac{M_{11}U(k_{z,s}, Z_s) + M_{12}U(-k_{z,s}, Z_s)}{M_{21}U(k_{z,s}, Z_s) + M_{22}U(-k_{z,s}, Z_s)} \quad (4.13)$$

Assuming that no wave is reflected back from the substrate if neutrons penetrate only a few microns, so that

$$U(k_{z,s}, Z_s) = 0 \quad (4.14)$$

Therefore the reflection coefficient is simply defined as

$$r = \frac{M_{12}}{M_{22}} \quad (4.15)$$

The transmission coefficient is defined as the ratio of the transmitted electric field to the incident electric field:

$$t = \frac{U(-k_{z,s}, Z_s)}{U(-k_{z,0}, Z_1)} \quad (4.16)$$

And is given by

$$t = \frac{1}{M_{22}} \quad (4.17)$$

This method of derivation of reflection and transmission coefficients is known as matrix technique. It is a general method which is valid for any electromagnetic wave [8].

4.4.2 Program Reflex13 graphical user interface

Program Reflex13 is user-friendly software that has a graphical user interface which allows easy interactions for less experienced users. Some software use programming language which is often

difficult to use for users who don't have a strong background in programming. This software is incorporated with Matlab and user has to type the following command: Reflex13, in order to get the graphical user interface (GUI) shown in Figure 4.2. Figures 4.3 and 4.4 are the main GUI for x-ray and neutron reflectivity, respectively.

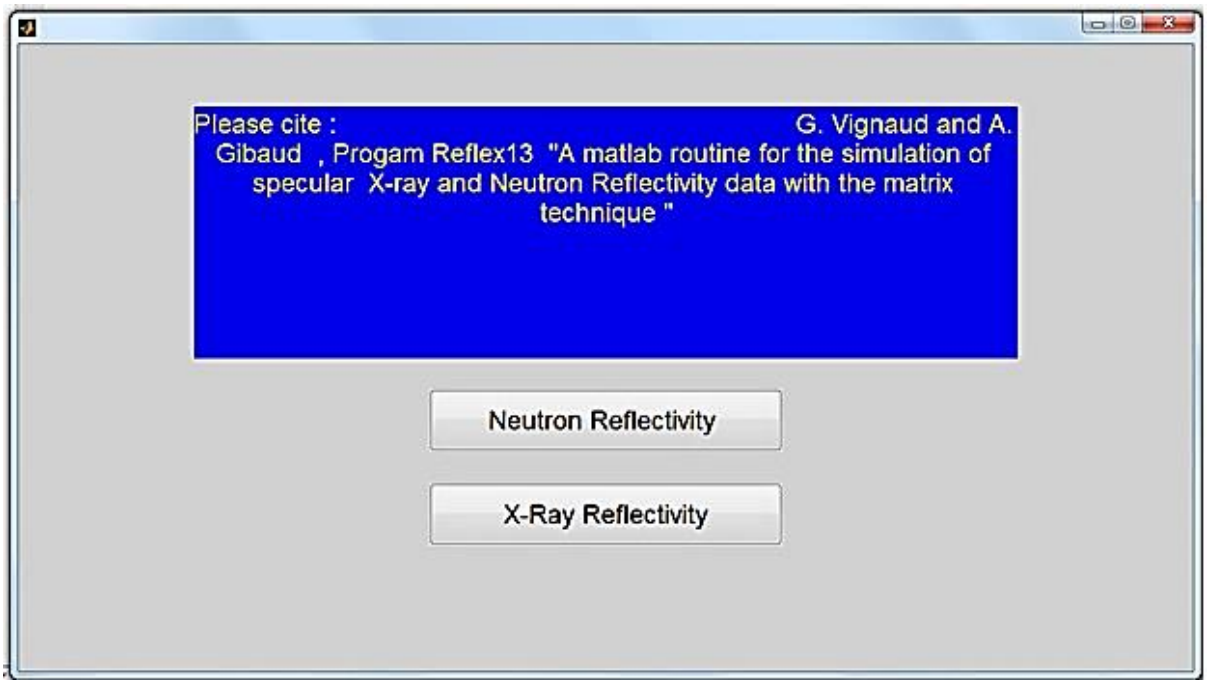

Figure 4.2: Screenshot of the initial graphical user interface after typing in the command: Reflex13,

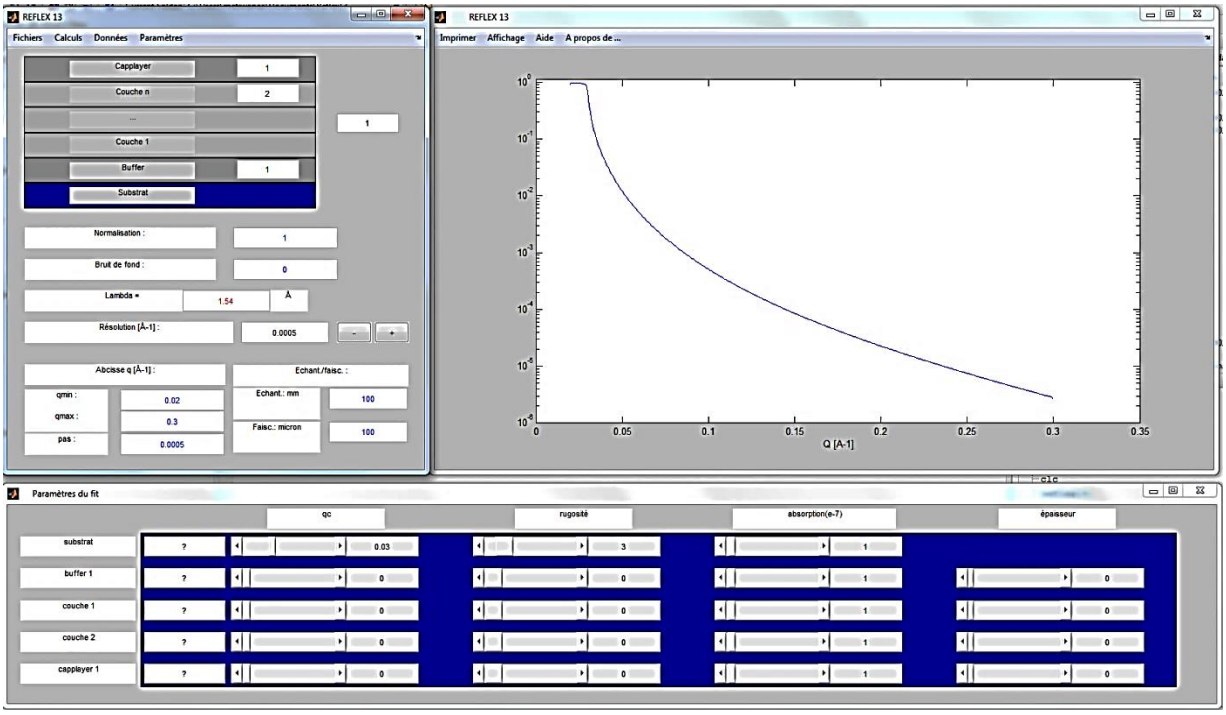

Figure 4.3: Screenshot of an X-ray reflectivity graphical user interface

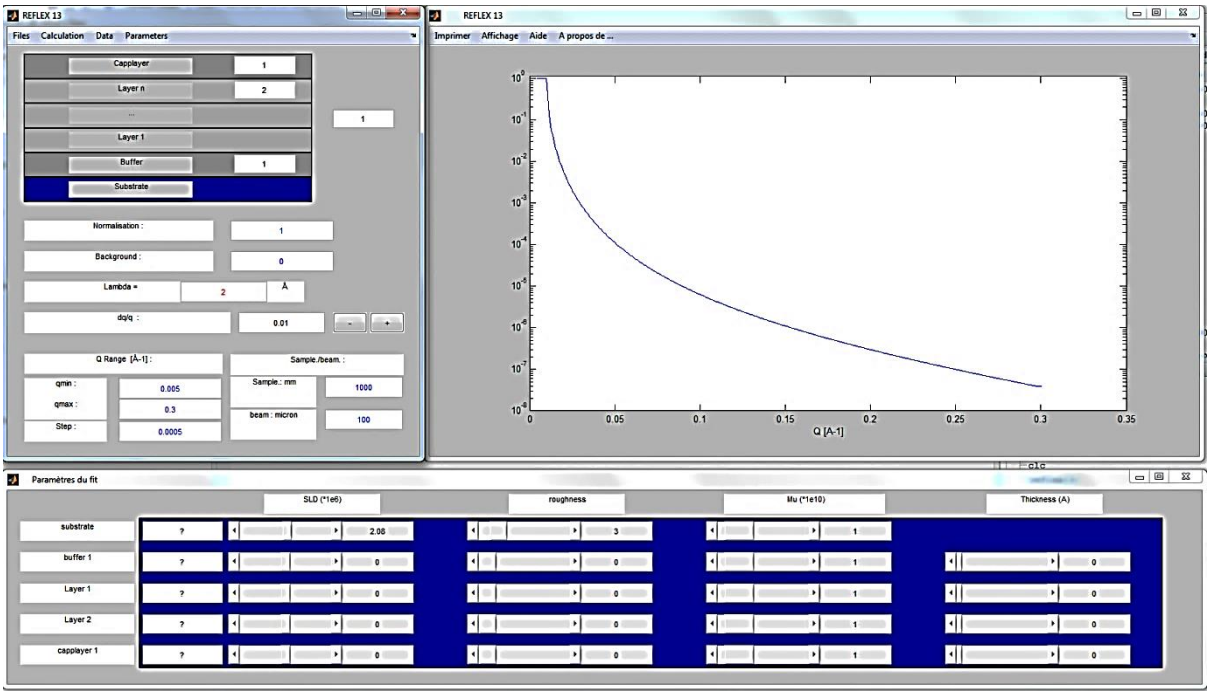

Figure 4.4: Screenshot of a neutron reflectivity graphical user interface

The GUI for X-rays and neutrons is almost the same. The only difference is that X-ray has an electron density while the neutron has a scattering length density. It is also important to mention that X-ray and neutron have different interactions. The main GUI for neutron reflectivity shown in Figure 4.4 comprises of different tabs. Many options including saving the reflectivity, load data file, export data files, simulated curves, and parameters. There are options to manually change the number of layers of the thin films and to include a buffer and/or capplayer between the layers of the thin films. Below that there's a tab for neutron wavelength in angstroms, and below wavelength tab, it's the angular divergence, dq/q, then there's a range and step to change your x-axis as one wish. Under the 'fit the parameters tab there are different parameters such as SLD, roughness, absorption denoted as (Mu), and thickness of any thin films under investigation.

4.4.3 Angular resolution ($\Delta\lambda/\lambda$, $\Delta\theta/\theta$)

It is important to consider the beam angular diversion and wavelength dispersion when simulating, the dq/q in the GUI (see Figure 4.4. The divergence of the incident beam is usually determined by two slits if the beam is smaller than the width of the sample 'seen' by neutron beam or by the slit and the sample if the sample is small enough to be illuminated by the beam. This divergence of incident beam has effects such as decreasing of the amplitude of the oscillations (kiessig fringes) and rounding of the continuity at the critical angle.

On the other side, wavelength dispersion is dependent on the monochromator or on the resolution time in the case of time-of-flight spectrometers. The effect of wavelength dispersion varies from that of angular diversion in this case the oscillations (kiessig fringes) disappear at high angles [9]. Improving the resolution gives better features of kiessig fringes and critical angle. However, high-resolution is not ideal as this narrows the angular width of reflectivity. Typical values for resolution for existing reflectometers range from 2% to 5%. All in all, it is good to adjust the resolution to match the expected thickness of investigated films. Thick films would require high resolution while thin films could be measured with a low resolution [10].

4.4.4 Neutron absorption

Neutron absorption is described by the imaginary part of the scattering length b. The absorption is negligible for thin films except for elements like gadolinium, samarium, and cadmium because these elements have (n, γ) nuclear resonance at thermal neutron energies which strongly increase

the absorption [10]. In Figure 4.4, the Mu (1*e10) is the absorption which is quite small and in the order of 10^{-10} . This affects generally the beginning of the curve [7].

4.4.5 Calculating SLD

Scattering length density (SLD), denoted as Nb, is the measure of the scattering power of a material. It increases with the density, how tightly packed scattering entities are as well as scattering power of the entities. In neutrons, the scattering length density arises from scattering length, b [11]. Since the software is GUI-based; it is important to know the SLD of different materials so that they can be fitted as parameters. SLD's can also be calculated using the following formula:

$$\rho \mathrm{N} = {}^{1}\!/_{\nu} \sum n_i b_i = \frac{\rho m \mathrm{N} A}{M} \sum \mathrm{n_i b_i} \qquad (4.18)$$

where ρm is the mass density, ν is the molecular volume, M is the molecular weight, n_i is the number of atoms and b_i is the scattering length of an atom.

4.4.6 Roughness

A thin film Fabry-Perot resonator cannot have a smooth surface/interface under non-ideal conditions hence the phenomenon such as roughness and interdiffusion affect it. The imperfectness of the interface/surface depends on the deposition process of the layers. Roughness is induced by the rough edges on the substrate and/or by grains when growing layers. Interdiffusion occurs between successive layers. This happens during the deposition of a top layer which is miscible with the bottom material [7].

4.4.7 Thickness

As mentioned before that a thin film Fabry-Perot resonator is comprised of two reflecting layers separated by a transparent layer, spacer layer. The thicknesses of these layers is of utmost importance in observing the neutron tunneling phenomenon, especially the transparent layer thickness as it is the one that's responsible for a number of tunneling resonances. All in all, these thicknesses play a crucial role in observing the tunneling phenomenon. This is discussed more in chapter 5.

4.4.8 Simulation environment

Program Reflex 13 can be used not only for analysis but also for the simulation of reflectivity profiles from parameters. In this case, a user doesn't need experimental data. This is where the above-mentioned equation, 4.18, can be used to calculate the scattering length densities. From then, one can input in other parameters such as the thickness of the thin films under investigation, the name of the material under investigation, the number of layers desired, the roughness of the layers and scattering length density as shown in Figure 4.5.

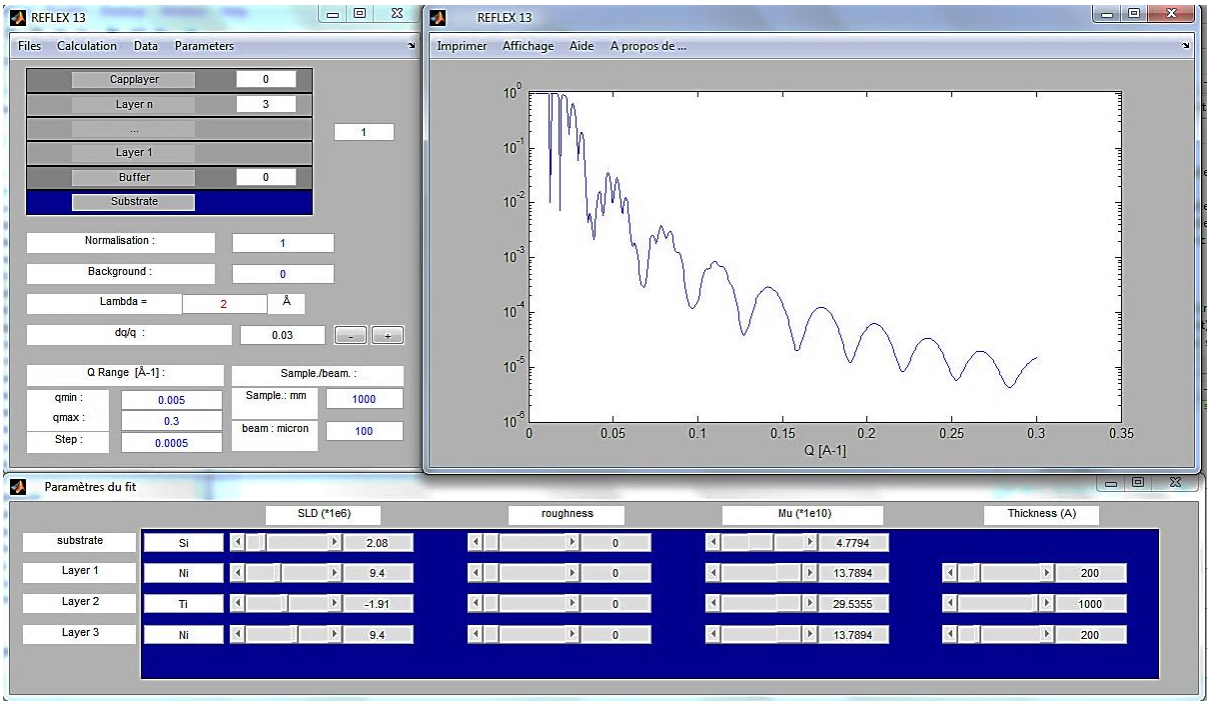

Figure 4.5: Screenshot of simulated curves of a thin film Fabry-Perot resonator of 200 Å Ni/ 1000 Å Ti / 200 Å Ni/Si on a silicon substrate.

In the simulation (see Figures 4.5 and 4.6), nickel and titanium are arranged in a geometry that resembles a Fabry-Perot resonator where two nickel layers are reflecting layers separated by a spacer layer of titanium. The thicknesses of two reflecting layers are kept at 200 Å while the thickness of the spacer layer, titanium, was 1000 Å. Equation 4.18 was then employed to calculate the scattering length density (SLD) of the reflecting layer and a spacer layer. It was found that the SLD of a transparent (spacer) layer and reflecting layers were -1.91 x 10^{-6}Å^{-2} and 9.4 x 10^{-6}Å^{-2} respectively. The roughness was kept at zero for reflecting layers and the spacer layer. All these parameters were fitted under 'Parameters du fit' in the program Reflex13 and

there was a calculated neutron reflectivity curve. In the calculated neutron reflectivity curve there are two regions: the first is the total reflection plateau, where tunneling resonances occur and it's the main feature of the thesis, the second region is called a vitreous region which is characterized by numerous kiessig fringes which are due to interference between waves reflected at air-Ni, Ni-Ti, and Ti-Si interfaces.

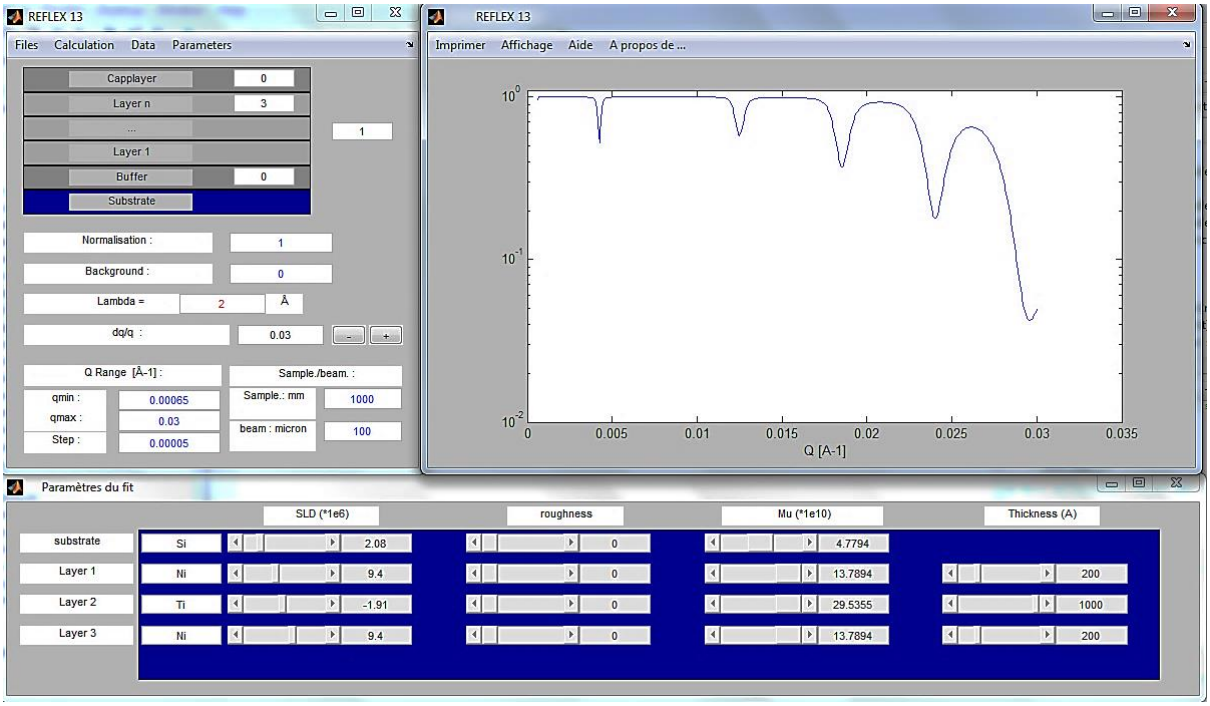

Figure 4.6 Zoomed in screenshot of simulated curve of a Fabry-Perot resonator like thin film of 200 Å Ni/ 1000 Å Ti/ 200 Å Ni/Si

The main feature, the total plateau of reflection, has also been identified, by zooming in, Figure 4.6, to observe clearly the sharp resonances that manifest to characterize the tunneling of neutron wave-particles. In order to identify the total reflection plateau, Q range in the x-axis can be changed to the desired range. Change minimum and maximum Q as well as the step. The resolution, dq/q, was kept at 0.03 which is 3% and it shows better features such the kiessig fringes critical angle

References

[1] W.D. Kelton and A.M.Law, "Simulation Modeling and analysis," McGraw-Hill, 1991.

[2] D.H. Withers, B.L.Nelson, S.Andradottir and K.J.Healy, "Proceedings of 1997 winter simulation conference," 1997.

[3] J.E. Freund, Mathematical statics,Fifth edition, Prentice-Hall, 1992.

[4] T.H. Naylor, J.L.Balinty, D.S.Burdick and K.Chu, Computer simulation technique, John Wiley, 1966.

[5] P. Colella , W.Group and W. D.Keyes, A science-based case for large-scale simulation, Science workshop, 2004.

[6] P. Bratley, B.L.Fox and L.E.Schrage, A guide to simulation, second edition, Springer-Verlag, 1987.

[7] A. Gibaud and G.Vignaud, "A Matlab routine for the simulation of specular X-ray and neutron reflectivity data with matrix technique," 2009.

[8] G. Vignaud and A.Gibaud, "Specular reflectivity from smooth and rough surfaces," *Lect.Notes Phys.*, vol. 770, p. 85-131, 2009.

[9] A. Menelle, F.Ott and C.Fermon, "Neutron Reflectometry," *Lect.Notes.Phys.*, vol. 770, p. 183-234, 2009.

[10] M.M. Demkowicz, "Probing interfaces in metals using Neutron Reflectometry," *Metals*, vol. 6, p.2-7, 2016.

[11] C. Bohren and D.Huffmost, Absorption and scattering of light by small particles, Wiley, 2004.

Chapter 5

Experiments, modeling, results, and discussion

5.1 Experiments

5.1.1 Synthesis of Nickel based isotopic thin films Fabry-Perot resonator

The isotope nickel thin film Fabry-Perot resonator like of ^{58}Ni – ^{62}Ni- ^{58}Ni on a silicon substrate was prepared by ion beam sputtering technique at a deposition temperature of 300 K from ^{58}Ni and ^{62}Ni targets. The distance between the targets and the substrate was fixed to 25 cm assuring thickness uniformity better than 1 % on a 2 x 2 cm area. The ion beam was extracted from a 3 cm diameter ion source. Prior to deposition, the system was pumped with a cryogenic pump down to a pressure of about 10^{-8} mbar while deposition was performed at $2x10^{-4}$ mbar. The ion beam was neutralized by injecting electrons with a hot tungsten filament. Ion beam sputtering was performed with argon of energy 1.2 keV and a current of 40 mA. The trilayer Fabry-Perot resonator was deposited on an optical surface quality undoped silicon substrates. Before the sputter, the substrates were sputtered etched several minutes. The rate of deposition was 1.5nm per minute for ^{58}Ni and ^{62}Ni. The layers' thicknesses were measured during deposition by a calibrated microbalance. In addition, a built-in soft x-ray reflectometer is used to control the periodicity of the stack. The main advantage of this double control, compared to the unique conventional quartz microbalance, for thickness monitor, lies in the self-compensation of thickness errors made on the successively deposited layers. One can note that this thickness control is very important in our case on a very small thickness fluctuation is tolerated to observe the so-called tunneling resonances. The targeted structure was 110 Å ^{58}Ni / 1000Å ^{62}Ni / 110 Å ^{58}Ni/Si.

5.1.2 Neutron reflectometry measurements

Unpolarized neutron reflectometry measurements were carried out at the ORPHEE reactor located at CEA-Saclay. The time-of-flight EROS reflectometer was used. The incident neutron de Broglie wavelength varied, approximately, from 3 to 25 Å. The grazing angle and relative angular resolution were of order 0.8˚ and 0.05 respectively. The theoretical simulation of the reflectivity profile is performed using the standard matrix method by assuming an ideal periodic structure with slightly rough interfaces and no thickness errors in the periodicity. In Figure 5.1 is the brief description of how EROS reflectometer operates. Neutrons produced by ORPHEE reactor are

thermalized by liquid hydrogen cold source at 20K. A neutron guide transports neutrons up to the spectrum situated around 30 m from the source. A beam containing broad wavelengths (3 – 25 Å) is then available at the chopper position. The chopper with a constant resolution is made up of two rotating wheels covered by a gadolinium, neutron absorber, pierced by two large slits. The distance and phase between two wheels enable one to change angular resolution from 1% to 13% depending on the request. In this study, it was 5%. The beam passes through a collimator under vacuum. The aperture of the horizontal entrance and exit slit may be changed from 0.2 mm to several cm. The beam is then reflected by a sample tilted of an angle and measure by a 3He detector [1].

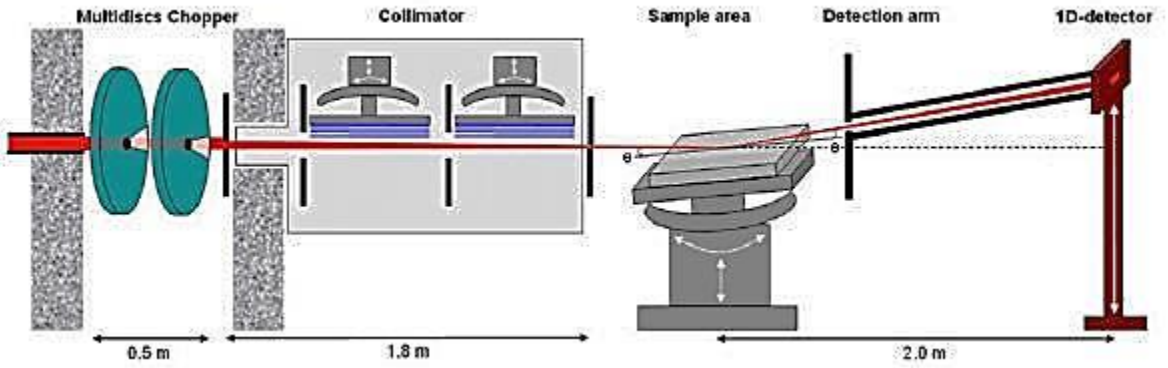

Figure 5.1 Schematic diagram of the EROS reflectometer employed in measurements of experimental data.

5.2 Modeling

5.2.1. Effects of thickness

The thickness of layers of the thin film Fabry-Perot resonator plays a role in assisting in the observation of the neutron tunneling phenomenon. A Fabry-Perot resonator is made up of two reflecting layers separated by a transparent layer, spacer layer, and it is a prerequisite to observe tunneling. A transparent layer thickness gives the number of tunneling resonances while reflecting layers' thicknesses either shifts the reflectivity profile to higher momentum wave vector transfer (Q) or lower momentum wave vector transfer (Q) by either decreasing or increasing the thicknesses. Program Reflex 13 software has a thickness as one of the parameters. Different thicknesses of the layers of thin film Fabry-Perot resonator were modeled to observe the behavior of the tunneling phenomenon, their effect on the tunneling phenomenon, and to also determine

which model resembles the experimental results. Below are some of the thicknesses that were modeled.

Program Reflex13 software has other parameters such as roughness and angular resolution. Their effects on the tunneling resonances are also explored.

5.2.2 Changing the thickness of transparent layer

Transparent layer, also known as a spacer layer, of a thin film Fabry-Perot resonator like plays a role in the manifestation of tunneling resonances in the total reflection plateau. Changing a thickness of a transparent layer affect the sharp dips. A decrease or increase in the transparent layer thickness causes the tunneling resonances, dips, either decrease or increase in numbers and in depth. When there's a constant decrease of about 100Å in the transparent layer thickness while keeping the reflecting layers' thickness constant, the tunneling resonances start to decrease in depth and they start to get less in numbers until all dips disappear at about 200 Å.

On the other hand, when there's a constant increase of the transparent layer thickness of about 100 Å each time, the tunneling resonances' depth is bigger and more new dips start to appear. When the transparent layer thickness reaches 2000 Å, the number of tunneling resonances increases from 3 to about 8.

5.2.3 Changing the thicknesses of reflecting layers

Unlike a transparent layer, changing a reflecting layer thickness doesn't have that much effect on the tunneling resonances. When the reflecting layers thicknesses is decreased by a constant of about 100 Å, the number of tunneling resonances stays the same. The sharp dips' depth gets longer which is likely due to neutrons passing with ease since the reflecting layer is thin enough. When this thickness is thin enough, roughly 100 Å, the number of tunneling resonances also drop from 3 dips to 2 dips and the reflectivity profile shifts to higher wave vector transfer.

The opposite occurs when the reflecting layers' thicknesses are increased. The depth of sharp dips gets shorter because the thickness is now thick and neutron wave 'spends' more time penetrating the thicker layer.

5.2.4 Specific changes in reflecting layers

150 Å ^{58}Ni / 1000 Å ^{62}Ni / 150 Å ^{58}Ni/Si

Increasing a reflecting layers thicknesses from 150 Å to 300 Å affects the depth of a dip, tunneling resonance. The increase in the thickness decreases the depth of a tunneling resonance. The width of a tunneling resonance stays the same. At higher thickness, 300 Å, tunneling resonances' depth gets shorter and reflectivity profile shifts to higher wave vector transfer. The decrease in dips' depth can be accounted by a denser thicker layer which makes a neutron 'stay' longer inside that layer.

The same trend is observed in natural thin film Fabry-Perot resonator like of nickel and titanium, 150 Å Ni / 1000 Å Ti / 150 Å Ni/Si. However, this system has more tunneling resonances than the isotope because titanium, which is responsible for tunneling resonances, has been used as the transparent layer and according to neutron optics it is the highest transparent material, it presents very low neutron absorption [2] but tunneling resonances of isotopic system, isotopic nickel thin film Fabry-Perot resonator like, are sharper and long depth than the natural system.

This trend has also been observed in the system that has isotopic reflecting layers and natural transparent layer, 150 Å ^{58}Ni / 1000 Å Ti / 150 Å ^{58}Ni/Si. The sharp dips decrease in depth as the reflecting layers' thicknesses increases. There's a shift towards higher wave vector transfer (Q).

5.2.5 Full width at half maximum and tunneling resonance spectral position

The full width half maximum and spectral positions of sharp dips with different reflecting layers' thicknesses were determined. When the reflecting layers' thicknesses were changed to 150 Å, the spectral position and full-width maximum of each depth of tunneling resonance increased as shown in Table 5.1. All these FWHM and spectral positions, from all Tables 5.1 to 5.3, were determined while reflectivity profile was changed in scale to focus in the place of interest, which is the total reflection plateau where neutron tunneling phenomenon manifests itself, Hence they keep increasing with increasing Q. In Table 5.2 the spectral positions and FWHM's for each dip increased as the momentum transfer wave vector (Q) increases and as the thicknesses were changed to 200 Å. The similar trend was observed in Table 5.3, when the thicknesses of reflecting layers were increased to 300 Å, the full width at half maximum and spectral position of each sharp dip increased. However, increase of reflecting layers' thicknesses from 150 Å to 200 Å to 300 Å

resulted in different spectral positions of the 3 sharp dips with long depth. When the reflecting layers were thicker the FWHM started decreasing. The spectral position of reflecting layers thicknesses at 300 Å decreased. This means that the sharp dips were 'shifting' to the lower wave vector transfer, meaning that as thicknesses increase, the shorter the dips get. Overall, increasing the reflecting layers' thicknesses from 150 Å to 300 Å decreases the full width at half maximum and spectral position of the sharp dips as depicted by Table 5.1 to Table 5.3. This exhibit the time of neutron wave-particles once inside the media.

Table 5.1 full width at half maximum and spectral position of tunneling resonances where a reflecting layers' thickness is 150 Å

150 Å ^{58}Ni / 1000 Å ^{62}Ni / 150 Å ^{58}Ni/Si

Tunneling resonance	**FWHM ΔQ_r (Å^{-1})**	**Resonance tunneling Spectral position Q_r(Å^{-1})**
Short tunneling resonance's depth	0.000553 Å^{-1}	0.0105 Å^{-1}
Medium tunneling resonance's depth	0.00107 Å^{-1}	0.0193 Å^{-1}
Long tunneling resonance's depth	0.00132 Å^{-1}	0.0263 Å^{-1}

Table 5.2 full width at half maximum and spectral position of tunneling resonances where a reflecting layers' thickness is 200 Å

200 Å ^{58}Ni / 1000 Å ^{62}Ni / 200 Å ^{58}Ni/Si

Tunneling resonance	**FWHM ΔQ_r (Å^{-1})**	**Resonance tunneling Spectral position Q_r(Å^{-1})**
Short tunneling resonance's depth	0.00053 Å^{-1}	0.0106 Å^{-1}
Medium tunneling resonance's depth	0.00085 Å^{-1}	0.0193 Å^{-1}
Long tunneling resonance's depth	0.0128 Å^{-1}	0.0262 Å^{-1}

Table 5.3 full width at half maximum and spectral position of tunneling resonances where a reflecting layers' thickness is 300 Å

300 Å ^{58}Ni / 1000 Å ^{62}Ni / 300 Å ^{58}Ni/Si

Tunneling resonance	**FWHM ΔQ_r (Å^{-1})**	**Resonance tunneling Spectral position Q_r(Å^{-1})**
Short tunneling resonance's depth	0.000572 Å^{-1}	0.0106 Å^{-1}
Medium tunneling resonance's depth	0.000859Å^{-1}	0.0193 Å^{-1}
Long tunneling resonance's depth	0.00106 Å^{-1}	0.0257 Å^{-1}

The full widths at half maximum and spectral position were determined from the Figures below. As seen from Figure 5.2, where the reflecting layers' thicknesses were 150 Å, all the 3 sharp dips have a different full width at half maximum and spectral position. In Figure 5.3 the reflecting layers' thicknesses was kept at 200 Å and it has the increasing full widths at half maximum. In Figure 5.4 the reflecting layers' thicknesses were kept at 300 Å. In all three Figures, it is observable that the number of tunneling resonances, the sharp dips, stays the same. This is due to the transparent layer's thickness that was kept constant at 1000 Å. The number of tunneling resonances depends on the transparent layer thickness. The thicker the transparent layer the more number of tunneling resonances.

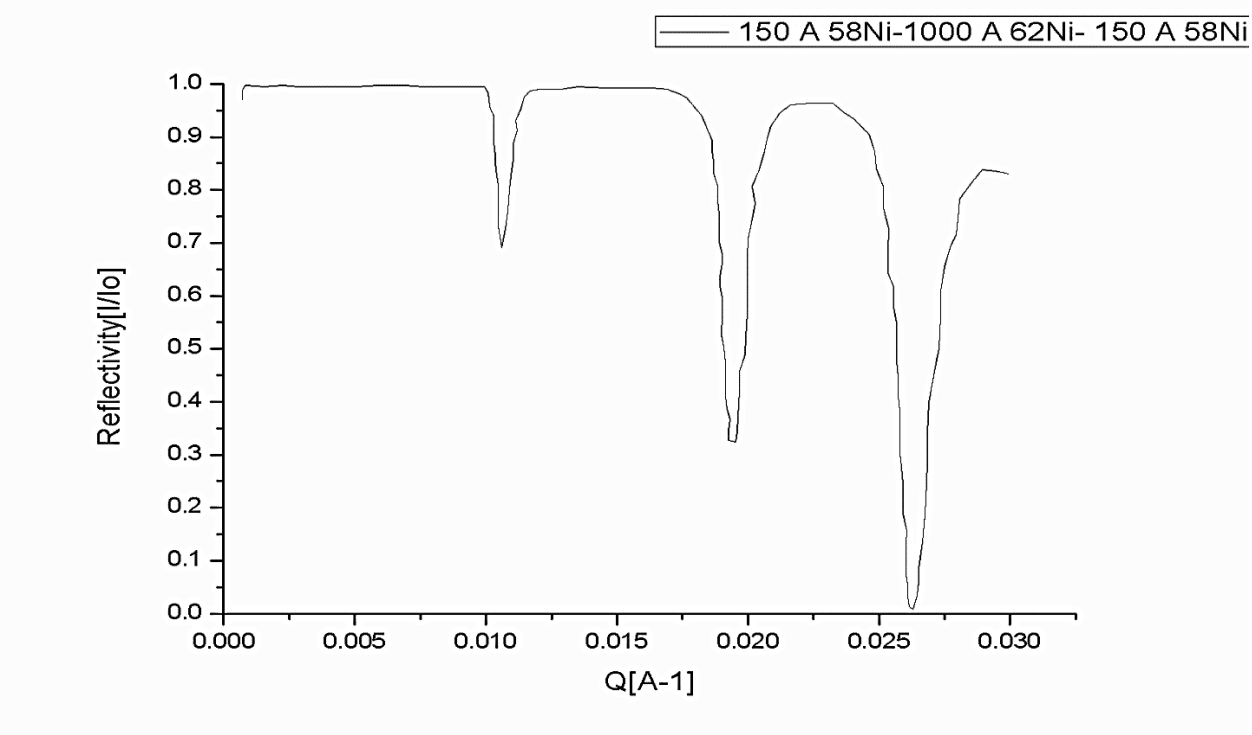

Figure 5.2 Reflectivity profile where the reflecting layers' thicknesses are 150 Å each layer.

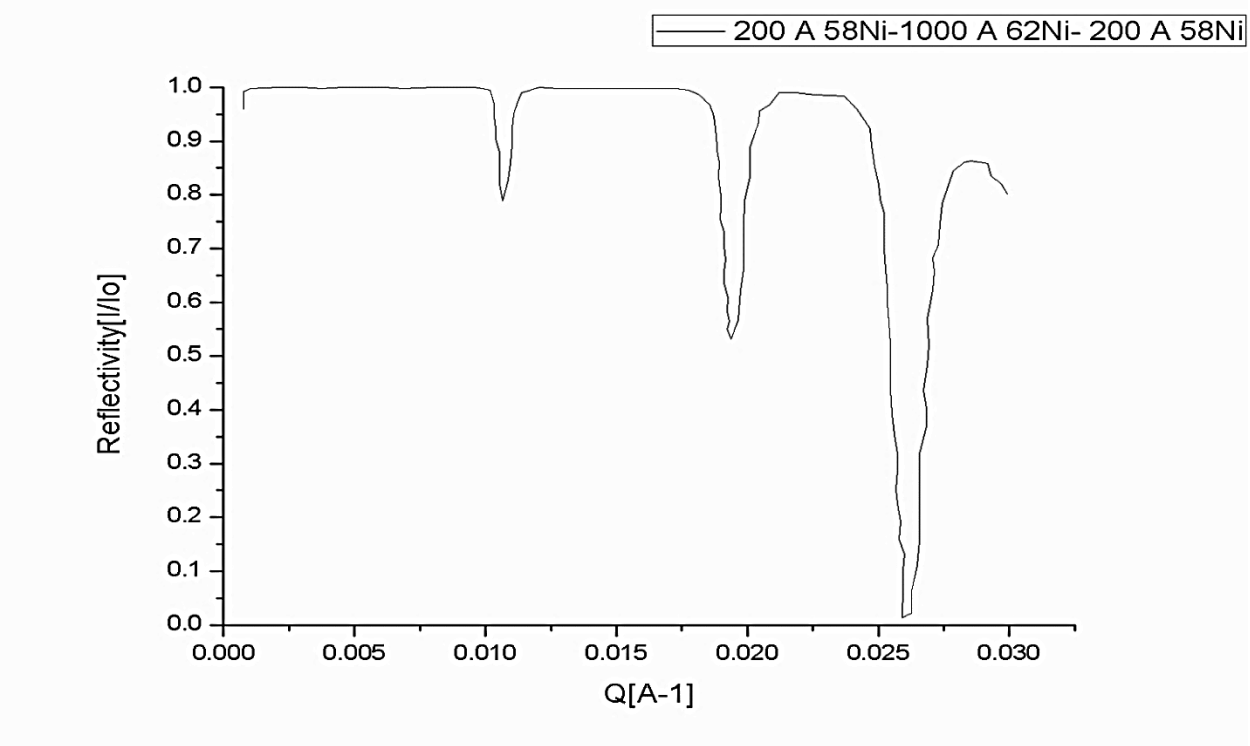

Figure 5.3 Reflectivity profile where the reflecting layers' thicknesses is 200 Å each layer.

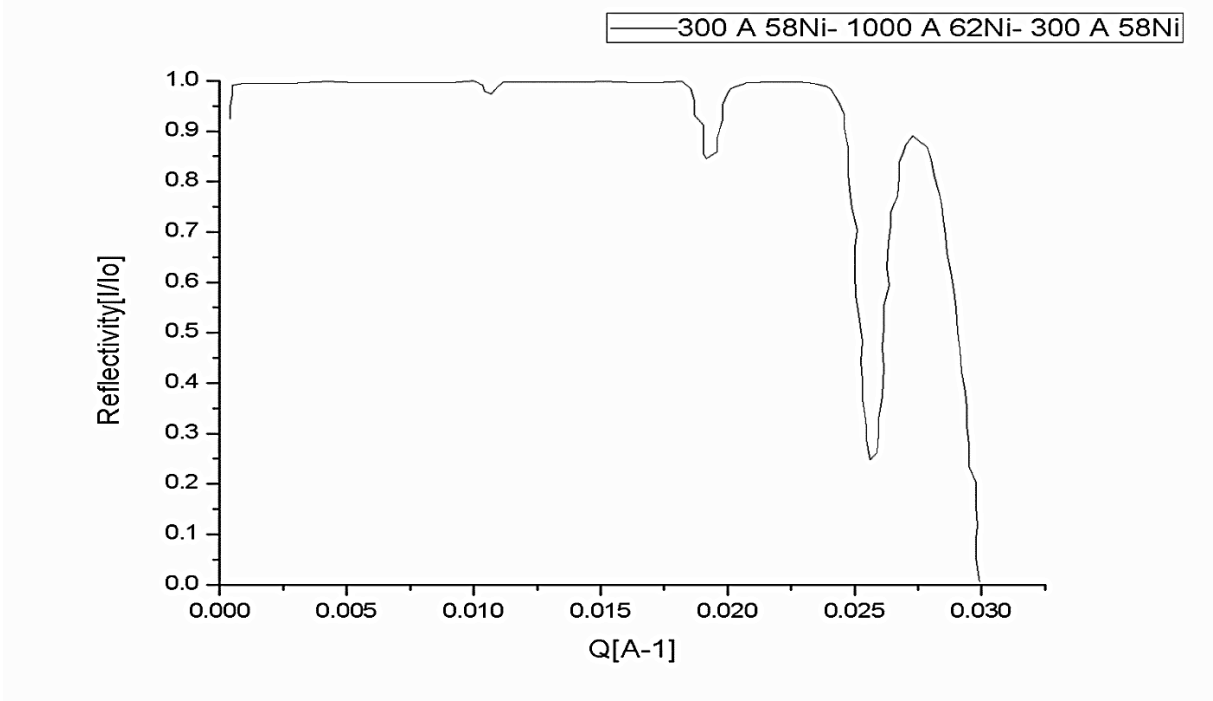

Figure 5.4 Reflectivity profile where the reflecting layers' thicknesses is 300 Å

5.2.6 Superimposed reflectivity profiles

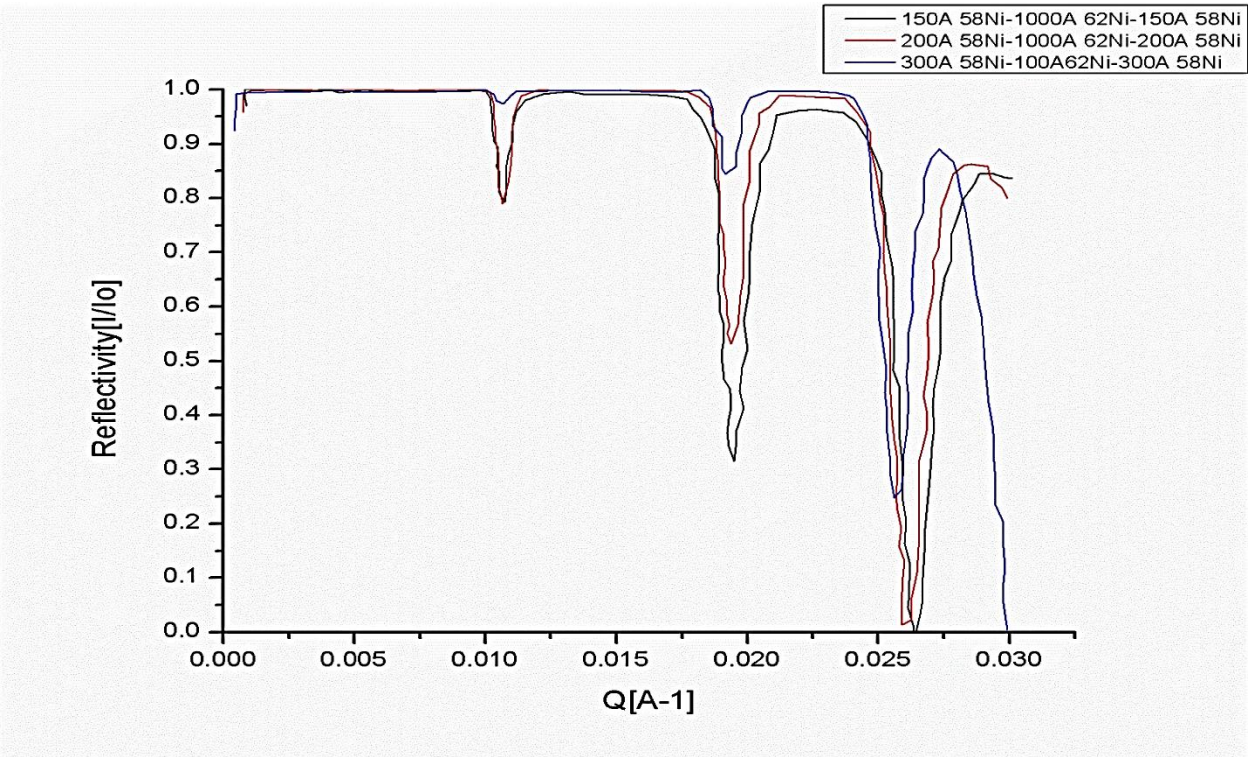

Figure 5.5 Superimposed profile reflectivities of different reflecting layer' thicknesses

When all three reflectivity profiles, as shown in Figure 5.5, with different reflecting layers' thicknesses, increasing from 150 Å to 200 Å to 300 Å, are superimposed then there's a clear distinction on the effect of reflecting layers thicknesses on the sharp dips, tunneling resonances, in the plateau of total reflection. As depicted, see Figure 5.5, the depth of sharp dips decreases as the reflecting layer thicknesses increase from 150 Å to 200 Å to 300 Å. Another observation is that the sharp dip that has longer depth, in all different thicknesses, shifts to the lower wave vector transfer as the reflecting layer thickness increases. This means that the thicker the reflecting layer thickness the harder for neutron wave to penetrate that layer since neutrons are weakly scattered once inside the media [3].

5.2.7 Natural material vs isotopic material

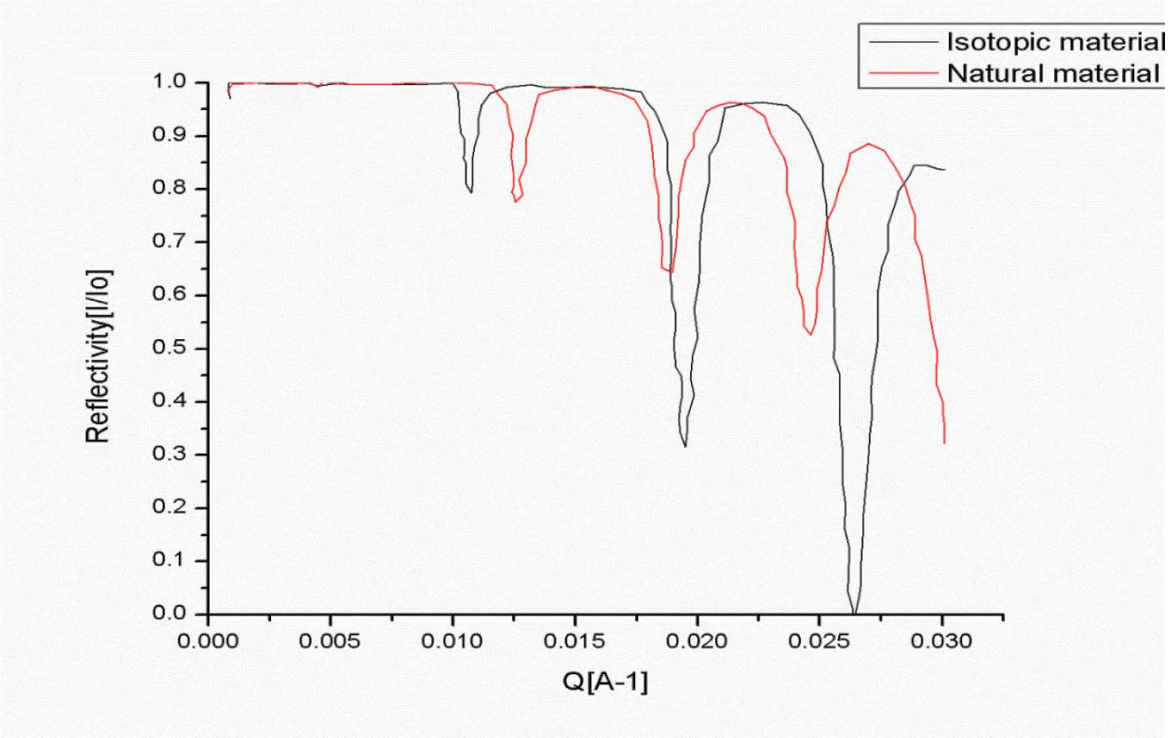

Figure 5.6 This Calculated reflectivity profile showing the difference between isotopic and natural material. The isotopic material that made up thin film Fabry-Perot resonator was in the following sequence: 150 Å ^{58}Ni / 1000 Å ^{62}Ni / 150 Å ^{58}Ni/ Si while the one for natural material was: 150 Å Ni / 1000 Å Ti / 150 Å Ni/Si.

A thin film Fabry-Perot resonator like is a prerequisite to observe the tunneling of neutron wave-particles. As said before, the geometry of this thin film Fabry-Perot device consists of two reflecting layers sandwiched by a spacer, transparent, layer. This thin film Fabry-Perot resonator

can be synthesized by isotope material or natural material. In this study, the isotopic material of nickel has been employed to observe neutron wave-particles suffering the frustrated total reflection, the tunneling phenomenon. In this case a natural material of 150 Å Ni / 1000 Å Ti / 150 Å Ni/Si is being compared to the isotopic material of 150 Å ^{58}Ni / 1000 Å ^{62}Ni / 150 Å ^{58}Ni/Si as shown in Figure 5.6. As depicted by the Figure 5.6, isotopic material, which the thin film Fabry-Perot resonator is like comprises of nickel isotope, have tunneling resonances that have long depths than the natural material meaning isotopes have tunneling resonances that are broad which is likely due to large scattering length of ^{58}Ni(b_c) = 14.4 fm. Natural material has tunneling resonances that are shifting towards the lower wave vector transfer. However, the natural material has more tunneling resonances, 4 tunneling resonances as compared to isotopic material which has 3. The reason for that is because the spacer layer of natural material is titanium, which is the highest transparent material according to neutron optics.

5.2.8 Effects of angular resolution

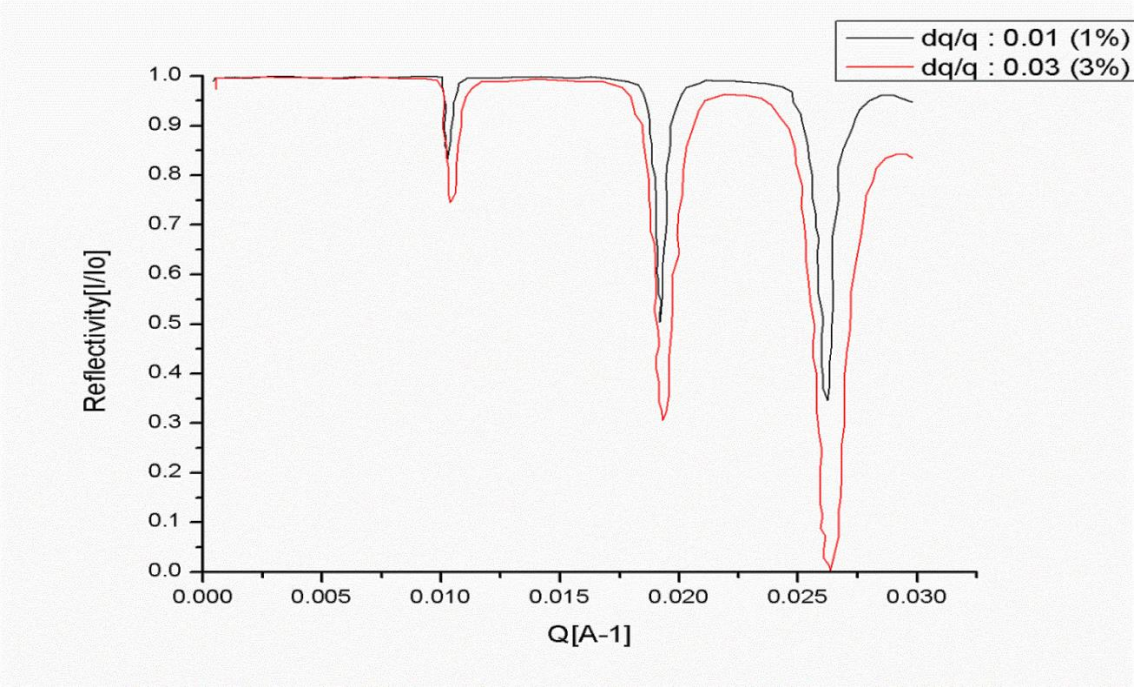

Figure 5.7 Reflectivity profiles showing effects of different resolutions employed. The thicknesses of both reflecting layers and a transparent layer were kept the same: 150 Å ^{58}Ni / 1000 Å ^{62}Ni / 150 Å ^{58}Ni/Si for both reflectivity profiles. Only resolution was changed.

It is of paramount importance to know about the angular resolution and it must be taken into account during the experiments and simulations. Typical resolution for existing neutron reflectometers ranges from 1% to 13%. A resolution of 2 % has an ability to distinguish between 2 thickness values which differ by 2%.

The effects of resolution in tunneling resonances arise in their widths. As the resolution is increased, from 1% to 3%, also the width of tunneling resonance increases, as shown in Figure 5.7. However, in the vitreous region, the resolution decreases the amplitude of the kiessig fringes and resolves the thicknesses. This trend is exhibited by all thin film Fabry-Perot resonator like, from all isotopic based to natural materials.

5.2.9 Single layers

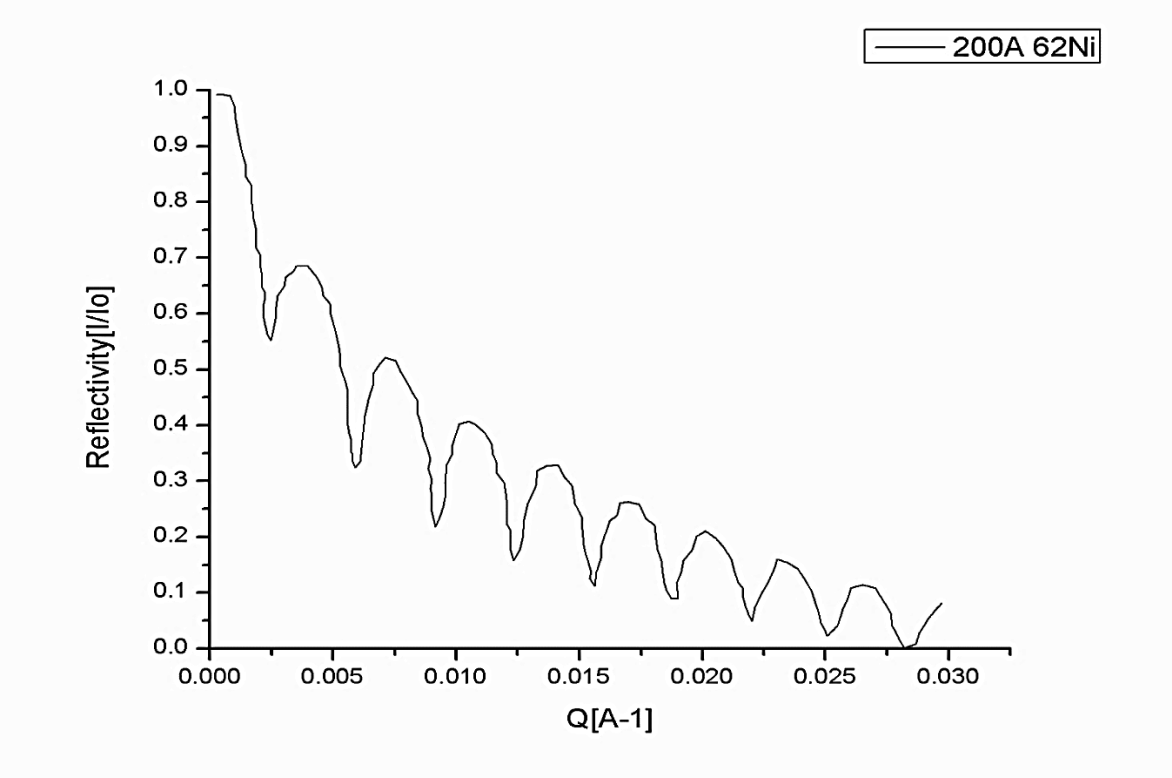

Figure 5.8 Reflectivity profile showing 200 Å of a transparent layer ^{62}Ni on a silicon substrate

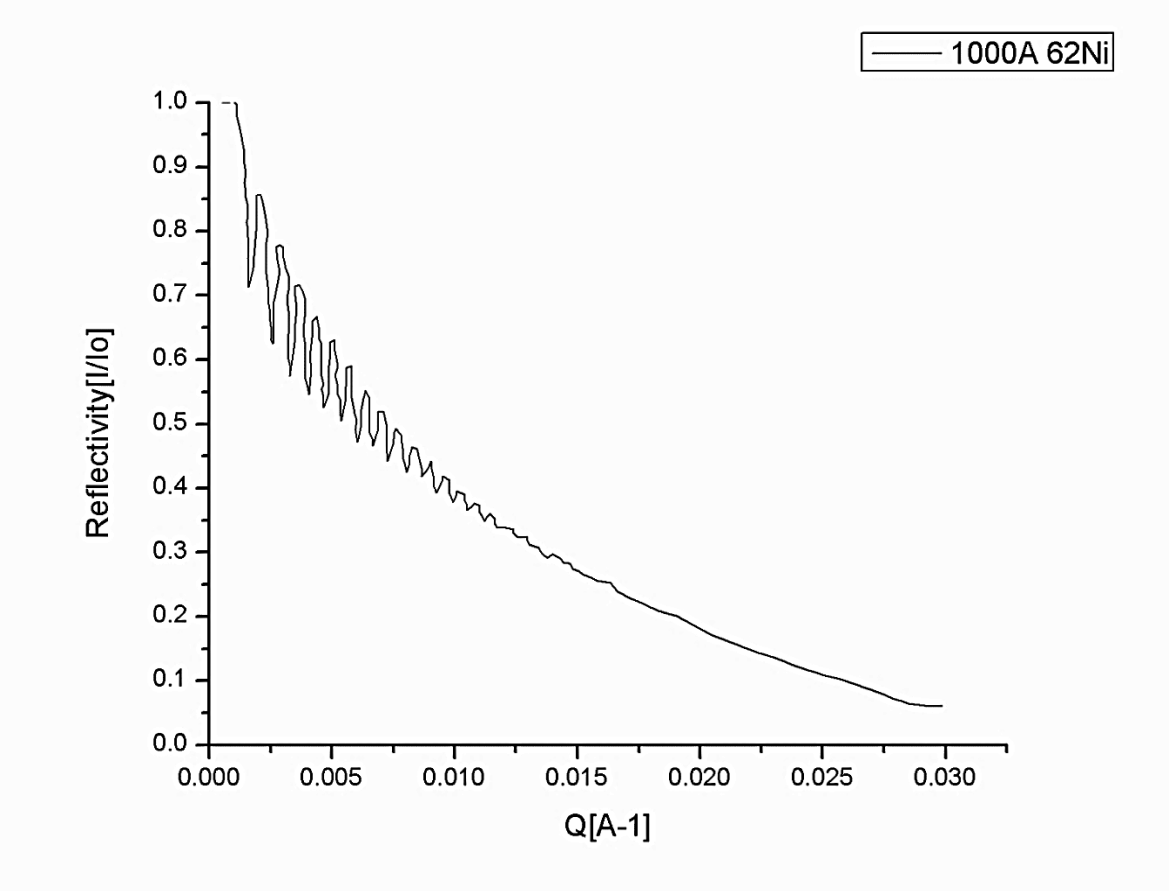

Figure 5.9 Reflectivity profile showing a transparent layer with 1000 Å thickness of ^{62}Ni on a silicon substrate.

A single layer of a material on a silicon substrate affects the Kiessig fringes in the vitreous region. If the single layer is thick then there will be numerous kiessig fringes, as depicted in Figure 5.8, and their interfringes decrease. On the contrary, if the single layer is thin, as shown in Figure 5.9, then there will be less kiessig fringes with their interfringes and amplitudes bigger. This is true for transparent and reflecting layers. This goes to show that neutron tunneling phenomenon occurs only in a thin film Fabry-Perot resonator where the geometry is a transparent layer sandwiched between two reflecting layers.

.

5.2.10 Effects of interfacial roughness

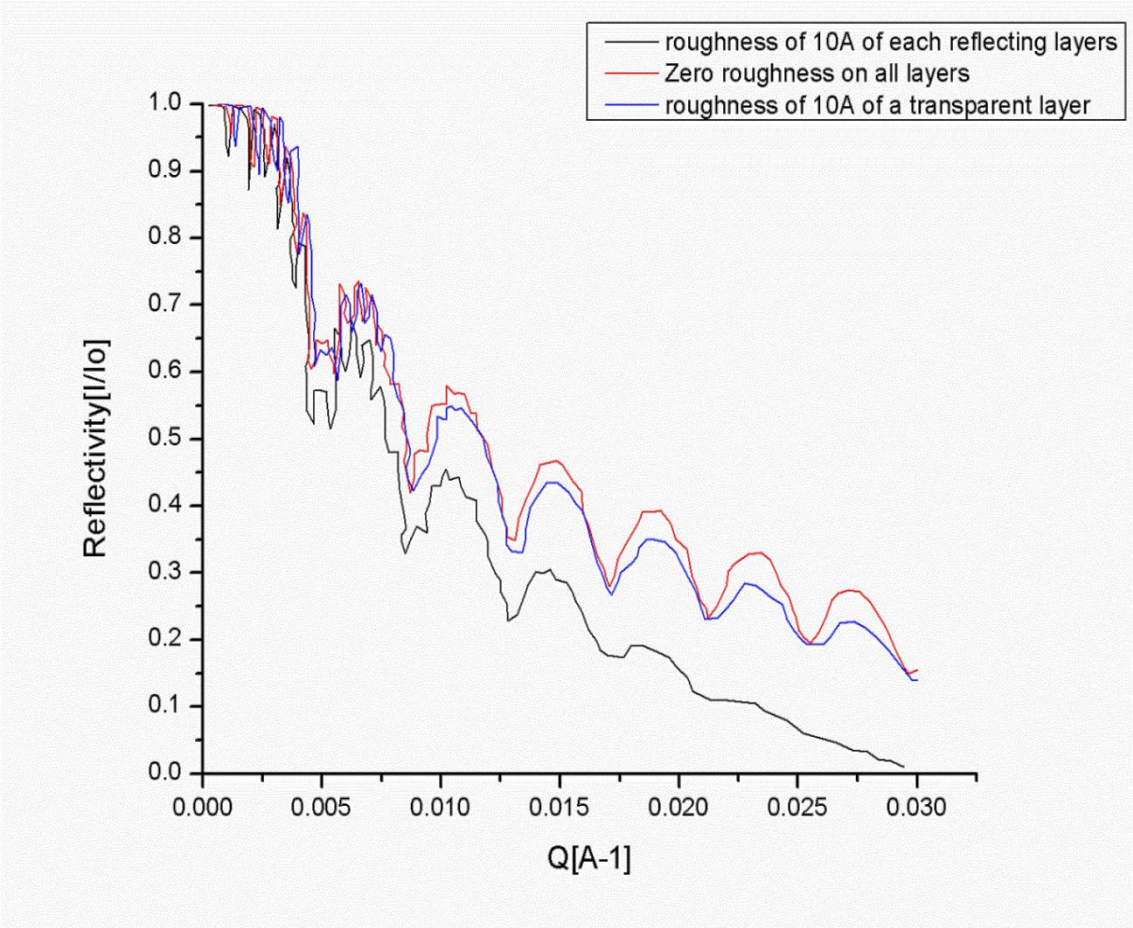

Figure 5.10 Superimposed reflectivity profiles of 150 Å ^{58}Ni / 1000 Å ^{62}Ni / 150 Å ^{58}Ni/Si with different interfacial roughness

The roughness of the interfaces doesn't have that much effect on the tunneling resonances in the total reflection plateau, which is the place of interest. Interfacial roughness affects the Kiessig fringes in the vitreous region. One starts to notice the shift to the higher wave vector transfer when the interfacial roughness is around 20 Å, which is the maximum roughness in the software. The increase of roughness of a transparent layer decreases the amplitude of the kiessig fringes and increases the interfringes. While the increase of roughness, of about 10Å, of reflecting layers reduces the amplitude of the Kiessig fringes and decreases the number of kiessig fringes as shown in Figure 5.10. It also smoothes out kiessig fringes at high momentum transfer vector.

.

5.3 Experimental results

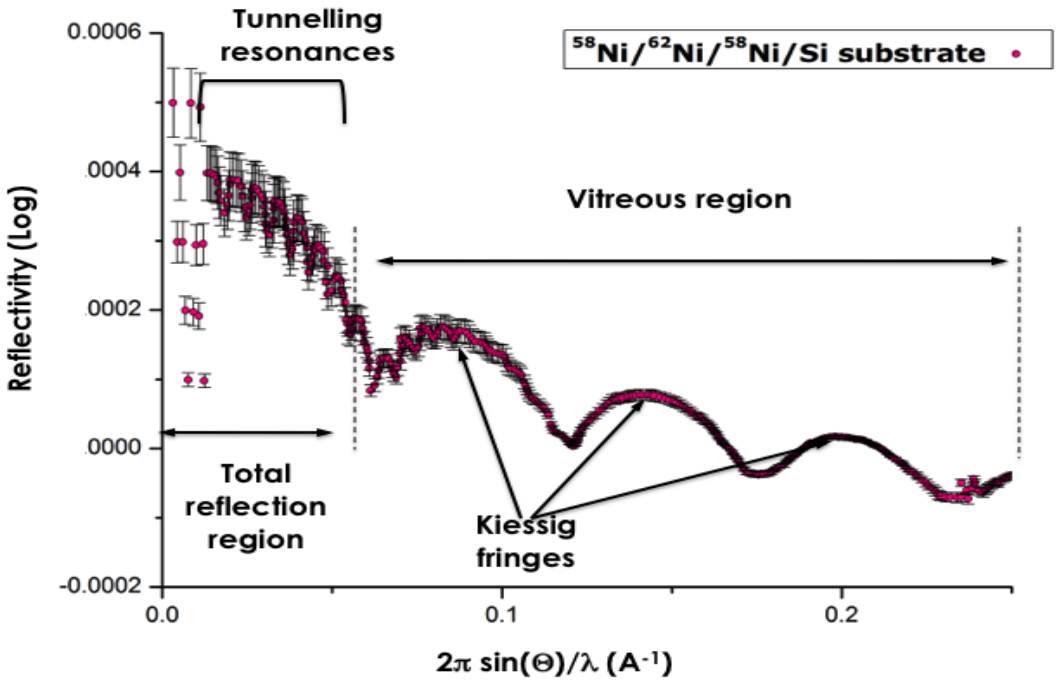

Figure 5.11 shows the experimental reflectivity profile of 110 Å ^{58}Ni / 1000 Å ^{62}Ni / 110 Å ^{58}Ni/Si

The neutron tunneling, frustrated total reflection, phenomenon in nanostructured isotopic nickel thin film Fabry-Perot resonator has been observed using unpolarized neutron reflectometry at grazing incidence angles. It manifested itself through sharp dips, tunneling resonances, in the total reflection plateau (region) [2]. In total 7 tunneling resonances, dips are observed, as depicted in Figure 5.11. The tunneling resonances, dips, in the total reflection plateau are due to tunneling phenomenon corresponding to quasi-stationary bounds of the neutron in the potential well formed by the nanostructured isotopic nickel thin film Fabry-Perot resonator. The number of tunneling resonances depends on the transparent layer thickness [4]. The oscillations present in the vitreous region are due to neutron wave-particle interference from the first reflecting layer and the buried interfaces of the nanostructured isotope nickel thin film Fabry-Perot resonator and they are called Kiessig fringes.

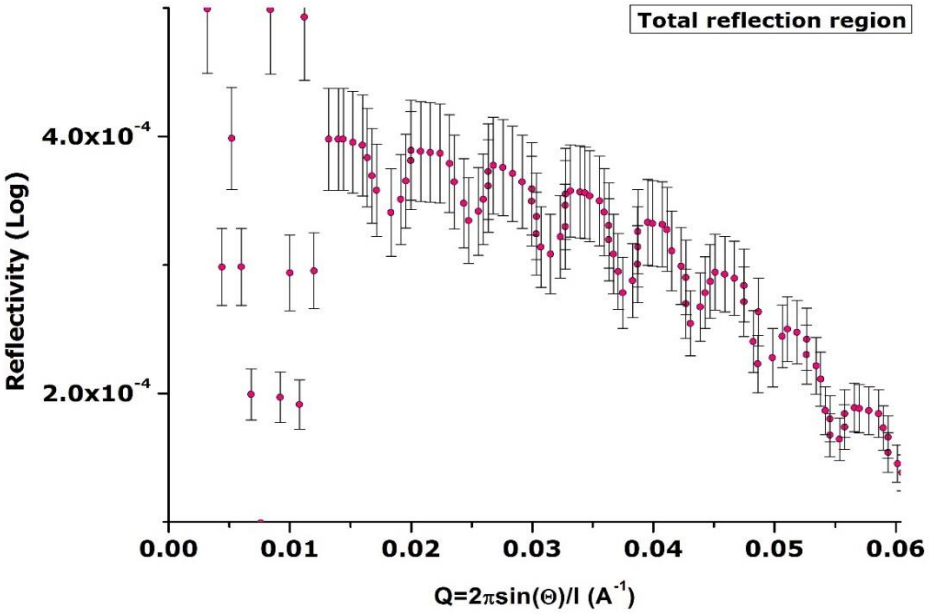

Figure 5.12 shows the total reflection region where tunneling phenomenon manifests itself

The total reflection region (plateau) is defined by momentum values smaller than the critical value Q_c of 0.058 $Å^{-1}$. Figure 5.12 shows clearly 7 tunneling resonances. The full width at half maximum (FWHM) and spectral positions of the tunneling resonances were determined. The full width at half maximum of these dips are different, the dips at lower momentum wave vector transfer (Q) have a larger full width at half maximum while at higher momentum wave vector transfer the FWHM is smaller, as depicted by Table 5.4. The dips' full width at half maximum decreases as the Q increases. This is correlated to the neutron lifetime in the nanostructured isotopic Fabry-Perot resonator [5].

Table 5.4 shows the full width at half maximum (FWHM) of the tunneling resonances, dips, and their corresponding spectral position

FWHM ΔQ_r ($Å^{-1}$)	**Resonance tunneling Spectral position Q_r($Å^{-1}$)**
0.00256 $Å^{-1}$	Q_1 : 0.0183
0.00215 $Å^{-1}$	Q_2 : 0.0247 $Å^{-1}$
0.00206 $Å^{-1}$	Q_3 : 0.0315$Å^{-1}$
0.00145 $Å^{-1}$	Q_4 : 0.0375 $Å^{-1}$
0.000875 $Å^{-1}$	Q_5 : 0.0430 $Å^{-1}$
0.0000955 $Å^{-1}$	Q_6 : 0.0486 $Å^{-1}$
0.00001599 $Å^{-1}$	Q7 : 0.0553 $Å^{-1}$

5.4 Comparing experimental results and simulated results

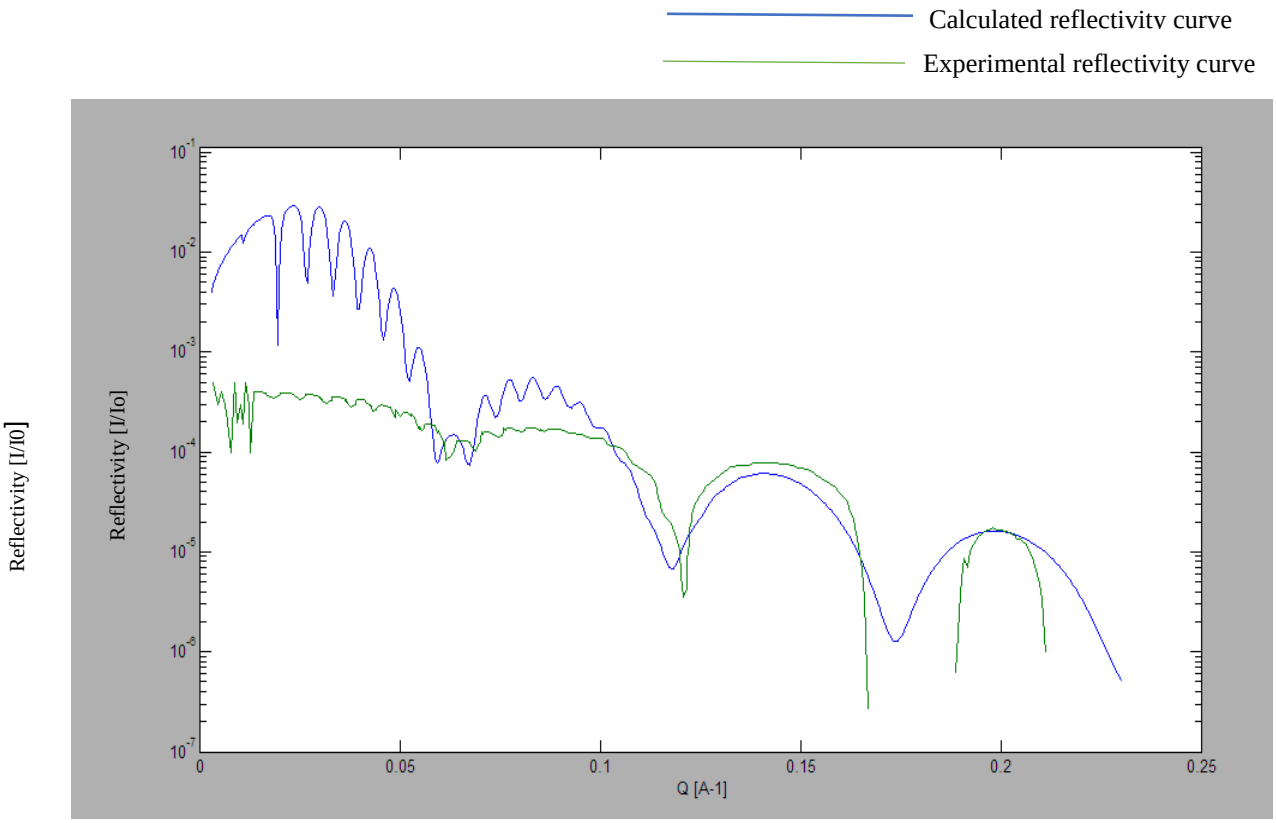

Figure 5.13: Experimentally obtained and calculated curves of unpolarized neutron reflectivity of 110 Å ^{58}Ni / 1000 Å ^{62}Ni / 110 Å ^{58}Ni/Si

Experimental results and theoretical (calculated) results have been compared. The dips in the experimental curve are not as sharp as the ones in the calculated curve; this is likely due to the angular resolution and/ or low intensity in this spectral range, once the neutron is inside the matter it loses intensity [3]. Neutron reflectometry measurements collect only the intensity of the reflected neutron beam [6]. From the analysis of experimentally obtained and calculated curves, it is possible to draw a conclusion about the agreement of experimental data and calculated curve, as depicted in Figure 5.13. The simulation of these curves was performed using program Reflex13 [7-9] .The simulation parameters employed are shown in Table 5.5 below.

Table 5.5: Parameters that were used in comparing the experimental reflectivity curve and calculated reflectivity curve

Parameter	**Value**
Reflecting layers' thicknesses	110 Å
Transparent layer thickness	1000 Å
Instrument resolution	0.03(3%)
Wavelength(lambda)	4.1 λ
Beam Width	1 mm
Sample	4.5 mm
^{58}Ni layer roughness	5 Å
^{62}Ni layer roughness	15 Å
^{58}Ni layer roughness	15 Å

References

[1] F. Cousin and A. Menelle, "Neutron reflectivity," *EPJ Web of Conferences,* Vols. 104, 01005, 2015.

[2] M. Maaza and D. Hamidi, "Nanostructured Fabry-Perot resonators in neutron optics & tunneling of neutron wave-particles," *Physics Reports,* vol. 514, p. 177-198, 2012.

[3] A.L. Frank, "Fundamental properties of neutron : Fifty years of research," *Sov.Phys.Usp.,* vol. 25, p. 280-297, 1982.

[4] M. Maaza, F.Bridou and B.Pardo "Tunneling Reflection with Polarized Slow Neutrons: Polarized-Neutron Total Frustrated Reflection," *J.Appl.Cryst.,* vol. 26, p. 327-333, 1993.

[5] M. Maaza, B.Pardo, J.P.Chaevinue, A,Raynal, A.Menelle and F.Bridou,"Neutron tunneling and neutron lifetime in a Ni-V-Ni Fabry-Perot thin film resonator," *Physics Letters,* vol. A223, p. 145-148, 1996.

[6] J. M.J. Demkowicz, "Probing Interfaces in Metals Using Neutron Reflectometry," *Metals,* vol. 20, no. 6, p. 2-8, 2016.

[7] G. Vigaud and A.Gibaud, "Program Reflex13, " a Matlab routine for the simulation of specular X-ray and Neutron reflectivity data with the matrix technique".

[8] G. Vignaud and A.Gibaud, "Specular reflectivity from smooth and rough surfaces," *Lect.Notes.Phys,* vol. 770, p. 85-131, 2009.

[9] A. Gibaud and J.Daillant, "X-ray and Neutron reflectivity:Principles and applications,," *Lect.Note.Phys.,* vol. 770, 2009.

Chapter 6

Conclusion and future work

6.1 Conclusion

The aim of this research project has been to observe the tunneling phenomenon of neutron wave-particles undergoing a total reflection in isotopic based nickel thin film Fabry-Perot resonator. The objective was to fabricate the isotopic based nickel thin film Fabry-Perot resonator and also to observe the tunneling phenomenon of neutron wave-particles undergoing total reflection in isotopic based nickel thin film Fabry-Perot resonator by unpolarized grazing incidence neutron reflectometry. In conclusion, tunneling phenomenon, 'frustrated' total reflection, of neutron wave-particles undergoing total reflection was observed in nanostructured isotopic based nickel thin film Fabry-Perot resonator. The isotopic nickel thin film Fabry-Perot resonator was made up of two highly reflecting layers of nickel-58 (^{58}Ni) separated by a transparent layer, spacer layer, of nickel-62 (^{62}Ni) deposited on a silicon substrate using ion beam sputter. The neutron reflectometry measurements were conducted by EROS reflectometer. The tunneling phenomenon of neutron wave-particles undergoing total reflection manifests itself via sharp dips, tunneling resonances, in the total reflection plateau due to quasi-bound states in nanostructured isotopic nickel thin film Fabry-Perot resonator. Reflex 13 software was employed, a Matlab routine for the simulation of specular X-ray and neutron reflectivity data with matrix technique, to simulate the behavior of the tunneling phenomenon, by using different values of the parameters such as the thickness, roughness of the interfaces, scattering length density of the material, thereafter experimentally obtained data and calculated (theoretical) data were compared. From the analysis of the comparison, it was possible to draw the conclusion about the agreement between the experimental data and the model proposed. A total of 7 sharp dips, tunneling resonances, were observed in the total reflection plateau to exhibit that the neutron tunneling phenomenon has manifested. The full widths at half maximum (FWHM) of these tunneling resonances decreased with increasing momentum wavevector transfer (Q). These correlate to the neutron lifetime in nanostructured isotopic nickel thin film Fabry-Perot resonator.

6.2 Future work

In a technological application, the future work intends to demonstrate the viability of totally isotopic based neutron optics devices. From a fundamental point of view, future work includes employing polarized grazing incidence neutron reflectometry, employing ultra-cold neutrons, so to investigate magnetic properties of nanostructured thin film Fabry-Perot resonator.